Optical Clearing for OCT Image Enhancement and In-Depth Monitoring of Molecular Diffusion

Kirill V. Larin, Mohamad G. Ghosn, Alexey N. Bashkatov, Elina A. Genina, Natalia A. Trunina, and Valery V. Tuchin

(Invited Paper)

***Abstract*—In this paper, we overview the basic principles, recent results, advantages, limitations, and future of the optical clearing method in application to many fields of biology and medicine. We also discuss the possibility of noninvasive assessment of molecular diffusion in tissues using the optical coherence tomography technique. Issues of safety and toxicity of application of different endogenous and exogenous molecules to tissues are outlined.**

***Index Terms*—Molecular diffusion, optical clearing, optical coherence tomography.**

I. Introduction

In THE visible and near-infrared wavelength range, the majority of tissues are low absorbing but highly scattering media. Scattering defines spectral and angular characteristics of light interacting with living objects, as well as its penetration depth. Thus, the deleterious effects of the optical properties of tissues and blood on light-based diagnostic and therapeutic techniques may be effectively mitigated by reducing light scattering. Optical clearing agents (OCAs) have been identified that can reversibly change the light scattering properties of tissues and blood. The challenge remains to elucidate optical clearing mechanisms and to identify properties of agents that are predictive of its optical clearing potential *a priori* [1], [2]. Moreover, functional imaging, monitoring, and quantification of diffusion of therapeutic, contrasting, and OCAs in fibrous and epithelial tissues (e.g., skin, sclera, cornea, dura mater, muscle, mucosa, etc.) *in vivo* as well as controlling of the tissue optical properties are extremely important for many biomedical applications.

The immersion technique has a great potential for noninvasive medical diagnostics using, e.g., optical coherence tomography (OCT) due to rather small thickness of tissue layers usually examined by the OCT, which allows for fast impregnation of a target tissue at topical application of an immersion agent. Usually, without optical clearing, human skin and the body's interior tissues, such as blood vessel wall, esophagus, stomach, cervix, colon, etc., can be imaged to a depth of about a few mm with OCT.

This paper aims to review the basic principles, recent results, advantages, limitations, and future of the optical immersion method as applied to clearing of the naturally turbid biological tissues and blood. The refractive index matching concept for enhancement of in-depth laser beam penetration into tissues and blood is discussed on the basis of *in vitro* and *in vivo* studies using the coherence-domain technique. The optical properties of tissues with basic multiple scattering, which are transformed to a low scattering mode, are analyzed. The enhanced diagnostic abilities of the method based on the improved contrast of abnormalities, on the increased in-depth profiling of soft and hard tissues, and on the monitoring of diffusion of endogenous and exogenous molecules within tissues are demonstrated.

I. Basic Principles of Tissue Optical Clearing and Mechanisms of Drug and OCAs Diffusion in the Tissue

In general, the scattering properties of a tissue (namely, the scattering coefficient μ_s and scattering anisotropy factor g) are dependent on the refractive index mismatch between cellular tissue components: cell membrane, cytoplasm, cell nucleus, cell organelles, melanin granules, and the extracellular fluid (ECF). For fibrous (connective) tissue (eye scleral and corneal stroma, skin dermis, cerebral membrane, muscle, vessel walls, female breast fibrous component, cartilage, tendon, etc.), the index mismatch of extracellular medium and long fibers of scleroprotein (e.g., collagen-, elastin-, or reticulin-forming fibers) is the origin of strong light scattering. The nucleus and the cytoplasmic organelles in mammalian cells that contain similar concentrations of proteins and nucleic acids have refractive indices that fall within a relatively narrow range (1.38–1.41) at a wavelength of 589 nm [3], [4]. The measured refractive index for

Manuscript received October 26, 2011; revised December 15, 2011; accepted December 15, 2011. Date of publication December 27, 2011; date of current version June 1, 2012. This work was supported in part by the Institute of Biomedical Imaging Sciences under Grant IBIS-97708, the NIH/NHLBI under Grant T32-HL07812, the AHA under Grant 11POST7430064, the Civilian Research and Development Foundation under Grant RUB1-2932-SR-08, and the National Science Foundation under Grant CMMI-0900743; in part by the Russian Foundation for Basic Research under Grant 10-07-00526-a; in part by the Grant 224014 PHOTONICS4LIFE of FP7-ICT-2007-2; in part by the Projects 1.4.09, 2.1.1/4989, and 2.2.1.1/2950 of the RF Ministry of Education and Science; in part by the RF Governmental Contracts 02.740.11.0484, 02.740.11.0770, and 02.740.11.0879; and in part by the FiDiPro, TEKES Program (40111/11), Finland.

K. V. Larin is with the University of Houston, Houston, TX 77204 USA (e-mail: klarin@uh.edu).

M. G. Ghosn is with the Baylor College of Medicine, Houston, TX 77030 USA (e-mail: ghosn@bcm.edu).

A. N. Bashkatov, E. A. Genina, and N. A. Trunina are with Saratov State University, Saratov 410012, Russia (e-mail: a.n.bashkatov@mail.ru; eagenina@yandex.ru; trunina1987@mail.ru).

V. V. Tuchin is with the Institute of Precise Mechanics and Control of the Russian Academy of Sciences, Saratov State University, Saratov 410012, Russia, and also with the University of Oulu, Oulu 8000, Finland (e-mail: tuchinvv@mail.ru).

Color versions of one or more of the figures in this paper are available online at http://ieeexplore.ieee.org.

Digital Object Identifier 10.1109/JSTQE.2011.2181991

the nuclei is $n_{nc} = 1.39$ [5]. The ground matter index (ECF or interstitial fluid) is usually taken as $n_0 = 1.35$–1.37 [3]. The scattering particles themselves (organelles, protein fibrils, membranes, and protein globules) exhibit a higher density of proteins and lipids in comparison with the ground substance and, thus, a greater index of refraction ($n_s = 1.39$–1.47) [3], [4]. The refractive index of the connective-tissue fibers is approximately 1.41 and depends on the hydration of collagen, its main component [6]. The refractive index of human blood plasma is approximately 1.33–1.35, depending on the wavelength [3]. The main scatterers in blood are red blood cells (RBCs). RBCs are cells without nuclei; they contain approximately 70% water, 25% hemoglobin (Hb), and 5% lipids, sugars, salts, enzymes, and proteins [7]. The refractive index of dry RBCs at a wavelength of 550 nm falls within a range of 1.61–1.66 [8]. A Hb concentration of 32 g/dL represents a typical Hb concentration within a human RBC, and the index of the solution is approximately 1.42 [9]. For physiological concentration of Hb in blood (14 g/dL), its refractive index is decreased from 1.369 to 1.352 at wavelength change from 400 to 700 nm [10]. For human whole blood, depending on the wavelength, the index is in the range of 1.36–1.40 [3].

The optical clearing technique is based on the impregnation of a tissue by a biocompatible chemical agent, which may have some hyperosmotic properties. The OCAs frequently used are glucose, dextrose, fructose, glycerol, mannitol, sorbitol, propylene glycol, polypropylene glycol, and polyethylene glycol (PEG) with different molecular weights, 1,3-butanediol, 1,4-butanediol, and their combinations, and X-ray contrasting agents (verografin, trazograph, and hypaque). There are a few main mechanisms of light scattering reduction induced by an OCA: dehydration of tissue constituents; partial replacement of the interstitial/ECF by the immersion substance; and structural modification or dissociation of collagen. The first mechanism is only characteristic for highly hyperosmotic agents. For fibrous tissue similar to sclera, dura mater, and dermis, the second mechanism is prevalent for all tested chemical agents because their molecule sizes are much less than the mean cross section of interfibrillar space. Both the first and the second processes mostly cause matching of the refractive indices of the tissue scatterers (cell compartments, collagen and elastin fibers) and the cytoplasm and/or ECF.

The refractive index matching is manifested in the reduction of the scattering coefficient ($\mu_s \rightarrow 0$) and increase of single scattering directness ($g \rightarrow 1$). For fibrous tissues, μ_s reduction can be very high. Structural modification can lead to tissue shrinkage—that is, to the near-order spatial correlation of scatterers and, as a result, the increased constructive interference of the elementary scattered fields in the forward direction and destructive interference in all other directions in regards to the incident light that may significantly increase tissue transmittance even at some refractive index mismatch [11]. For some tissues and for the nonoptimized pH of clearing agents, tissue swelling may take place that could be considered as a competitive process in providing tissue optical clearing [11]–[13]. The optical clearing process in collagen-based tissues may involve a change in the supra-molecular structure. Collagen reversible solubility in sugars and sugar alcohols may take place. Agent-induced destabilization of collagen structures may lead to an additional reduction of optical scattering in tissue owing to smaller size of the main scatterers [14].

For the use of hyperosmotic agents, osmotic pressure may play a significant role. On one hand, the osmotic pressure causes the generation of fluid flows and controls intensities of these flows; however, on the other hand, rather strong osmotic pressure may destroy tissue structure. This is a major physicochemical mechanism of OCA toxicity.

Not only soft but also hard tissues could be effectively cleared, which opens the way for the development of the least-invasive techniques for laser diagnostics and therapy of brain and other soft tissue hidden under bone, cartilage, or tendons. For example, optical immersion clearing of the cranial bone under action of anhydrous glycerol was investigated [15]. It was shown that exposure of a cranial bone sample for 1 h causes the decrease in reduced scattering coefficient of superficial tissue layers by approximately 25% at the wavelength range of 1400–2000 nm. In this case, the main role in the clearing process is the replacement of fluid in the extracellular space by the immersion substance, owing to the cranial bone structure having a rather high porosity [15].

Blood immerses or goes through practically all tissues, and its scattering properties are very strong and anisotropic; thus, its clearing is of great importance. The refractive index mismatch between erythrocyte cytoplasm and blood plasma, as well as specific size and structure, define the scattering properties of blood [3]. The refractive index of erythrocyte cytoplasm is defined mostly by Hb concentration [16]. The volume and shape of a single erythrocyte are defined by blood plasma osmolarity. Blood scattering also depends on aggregation or disaggregation capability of RBCs [17]. For hematous tissue, such as the liver, its impregnation by solutes with different osmolarity also leads to refractive index matching and reduction of scattering coefficient, but the effect is not so pronounced as for fibrous tissues which change size as a result of osmotic stress [11]. Upon introduction of OCAs into blood, the refractive index of the blood plasma increases and becomes comparable with that of RBCs. For example, when 6.5% glycerol solution was added to whole blood diluted by saline to twice its volume, the optical penetration depth at 820 nm was correspondingly increased by 17%. For the other tested agents (glucose, dextrans, propylene glycol, and trazograph), the enhancement of penetration was around 20–50% [11], [17]. It was shown that minimal light scattering occurs at a glucose concentration in blood of 0.65 g/mL. In this case, blood is totally immersed. However, residual scattering remains due to differences in spectral dependences of refractive indices of glucose solution and RBCs [17]. Evidently, such large concentrations of glucose could only be applied locally and for a short time to avoid damage to blood cells and vessel wall tissue. However, the use of endoscopic optical imaging techniques (OCT or confocal microscopy) and controllable injection of small amount of glucose in the vessel lumen can help to image an atherosclerotic plaque through a bloodless layer with a high contrast. There is also the possibility of applying a small amount of Hb, which could be released owing to local hemolysis

of RBCs within the vessel area nearby endoscopic optical probe as an immersion agent [18]. A 30–40% reduction of the scattering coefficient of blood in the spectral range 400–1000 nm due to the local hemolysis (up to 20% of RBC in the close vicinity of optical probe) was demonstrated theoretically [18] as well as experimentally [19].

Development of noninvasive methods for functional monitoring and quantification of molecular transport in epithelial and fibrous tissues *in vivo* and controlling of tissue optical properties are extremely important for many biomedical applications including therapy, diagnostics, and advanced imaging of various diseases. Successful management of these diseases requires long-term treatment with drugs; however, despite numerous investigations related to delivery of drug and cosmetic substances into human tissues and to control of the tissue optical properties, the problem of estimating diffusion coefficient of the drugs and various chemicals in tissues has not been studied in detail. Knowing the diffusion coefficients is important for the development of mathematical models describing interactions between tissues and drugs, in particular for evaluation of the drug's and metabolic agent's delivery through the tissue.

Many biophysical techniques for studying the permeation of various chemicals through biological tissue and estimation of the diffusion coefficients have been developed over the last 50 years. These methods are based on fluorescence, spectroscopic, Raman, photoacoustic, radioactive labeling, or nuclear magnetic resonance. Other measurements were based on monitoring the temporal changes of the scattering properties of a tissue caused by dynamic refractive index matching, including interferometric techniques, and OCT.

Many of these diffusion studies were conducted on dermatological tissues. Skin covers an area of approximately 2 m^2 in human and provides the major contact to the external environment. It prevents the loss of water and the ingress of foreign materials. The skin is a very heterogeneous membrane, but the layer that controls absorption is the outermost layer, the stratum corneum. The stratum corneum is only 10–20 μm thick but provides a very effective barrier to penetration. The exact nature of the barrier function has been investigated over many years and recent advances in biophysical techniques have provided interesting insights into the mechanisms of absorption at a molecular level.

At the same time, despite numerous investigations, the exact mechanism of skin penetration is unclear. There are a number of routes by which a molecule can cross the stratum corneum: these are intercellular, transcellular, and appendageal (through either the eccrine (sweat) glands or hair follicles) [20]. Under normal conditions, the appendageal route is not thought to be very significant; in part this is due to the low surface area occupied by the appendages. It is more difficult to determine differences between the transcellular and intercellular routes [21]. Although the transcellular route was initially considered most likely, it appears that, for most compounds, the intercellular route predominates. The transcellular path requires that transport occurs through the densely packed keratin-filled corneocytes and that multiple transfers between these cells and the lipid-filled intercellular channels take place. However, it has been demonstrated that access to the corneocytes is limited or precluded and the evidence points strongly to the intercellular route as the predominant pathway [22], [23].

The principal parameters, which control the penetration kinetics of chemicals across the skin, are [23]: 1) oil–water partition coefficient and solubility parameters; 2) molecular size and shape; 3) polarity and charge. Since the oil–water partitioning characteristics of a chemical are crucial to its ability to penetrate the skin [22], the lipid solubility is an important factor for percutaneous absorption too. However, because the epidermal layers beneath the SC are aqueous in nature, it follows that a penetrant must also exhibit measurable water solubility in order to permeate through to the dermal microcirculation. The oil–water (e.g., octanol–water) partition coefficient K_o/w may be defined as follows: $K_{o/w} = S_{\mathrm{oil}}/S_{\mathrm{water}}$, where S_{oil} and S_{water} are chemical saturation solubilities in oil and water, respectively. Because the partition coefficient is the ratio of solubilities, $K_{o/w}$ of 2, for example, can also be exhibited by a molecule which is very insoluble in both oil and water. It follows that such a compound will be capable of developing only a very small driving force across the skin, and will penetrate rather slowly. The solubility parameter may give an indication of compounds, which are likely to dissolve well in the SC lipids.

Molecular weight (MW) and hence the size of molecules of drugs and OCAs also contribute to the chemicals penetration into skin. However, since the MWs of most of used chemicals are in the range of 100–1000 Daltons, few-fold spread MW is relatively small compared to a very broad (several orders of magnitude) span of oil–water partition coefficients and lipid solubilities. For this reason, it can be assumed that MW is likely to involve a second-order effect compared to partitioning and solubility.

Since polar molecules are poor penetrants through the lipophilic SC, for the design of effective OCAs the chemicals should be have low MW of very polar hydroxyl and amine groups.

The total permeability coefficient across human epidermal membrane can be defined by $P_T = 1/((1/P_p + P_L) + (1/P_{\mathrm{epi}}))$, where P_T is the total apparent permeability coefficient, P_{epi} is the permeability coefficient across the viable epidermis, P_p is the pore pathway permeability coefficient, and P_L is the permeability coefficient of the lipoidal pathway. P_p and P_L represent the parallel transport pathways across SC [24]. For homogeneous membrane, the permeability coefficient P is related to the diffusion coefficient D by the following formula: $P = DK/l$, where K is the partition coefficient and l is the thickness of the tissue across which permeation is measured [25]–[27]. On the other hand, the general expression for the permeability of a molecule diffusing through a porous membrane is $P = \varepsilon D_r/\tau l$, where ε and τ are the porosity and tortuosity of the diffusional pathway, respectively, and D_r is the diffusion coefficient of the permeant in the membrane [28]. The parameters ε, τ, and l characterize the properties of the membrane. D_r is a function of both the solute and membrane characteristics and can be expressed as the product of the free diffusion coefficient of the solute in a solution and the diffusional hindrance factor $F(\lambda)$ where λ is the ratio of the hydrodynamic

radius of the solute and the effective pore radius of the membrane. The hindrance factor is a well-characterized function and has been reviewed by Deen [29]. If $\lambda \leq 0.4$, the hindrance factor can be expressed as $F(\lambda) = (1-\lambda)^2 (1 - 2.104\lambda + 2.09\lambda^3 - 0.95\lambda^5)$.

Functional imaging, monitoring, and quantification of diffusion of therapeutic, diagnostic, and OCAs and drugs in epithelial and fibrous ocular tissues (e.g., cornea and sclera) *in vivo* as well as controlling of tissue optical properties are extremely important for many biomedical applications including therapy and diagnostics of various devastating diseases of the eye, such as diabetic retinopathy and glaucoma. An efficient treatment of these diseases requires a proper selection and effective delivery of therapeutic agents.

The sclera is a connective tissue which, together with cornea, forms the outer coat of the eye. Transport properties of the sclera are of interest in relation to the transport of drugs applied topically into the eye. This includes diffusion of drugs across the conjunctiva and sclera to the anterior segment structures and of drugs applied directly to the scleral surface. It is also of potential relevance to delivery of drugs to the posterior pole in the treatment of posterior segment diseases [30]. The diffusional properties of the sclera are dependent on components of the scleral matrix. This consists mostly of collagen type I (the major collagen of the sclera), while collagens type III, type V, type VI, and type VIII account for less than 5% of the total collagen. It should be noted that the ratio of conjunctiva to corneal permeability in the human eye is about 100 [31] and the ratio of permeability of scleral to corneal stroma is 5–15 [30]. Solute size has a more pronounced effect on scleral than corneal permeability so a 16-fold difference in scleral permeability was noted when comparing insulin with sucrose, versus an eight-fold difference for the cornea [32]. In general, in the scleral tissue both diffusion and partition coefficients decreased with increasing MW and the partition coefficient is increased with increasing scleral hydration [30].

Mineralized bone tissue contains significant water fraction, which for cancellous bone amounts up to 20% of its wet weight [33]. However, skeletally mature cortical bone is a denser material in which the fraction of water is reduced to ~10% [34]. The fractional water content in bone remains similar across species for the same type of bone; however, within a single species it varies with age, sex, etc.

Water in bone may be found associated with the mineral phase, bound to the organic phase (collagen and cement substance) or free (bulk water). Bulk water fills the pores of the calcified matrix, which form a network of interconnecting channels, which communicate the bone vascular system with the osteocytes, embedded in the mineralized matrix. This communication network serves for the transport of nutrients, waste products, and signaling molecules from the vascular system to the osteocytes and vice versa. The water channels are also the transport pathways for calcium and phosphate ions flowing in and out of bone tissue, which act as a mineral reservoir for the rest of the organism [35].

Diffusion of substances in a porous composite material such as the calcified matrix of cortical bone takes place along the fluid-containing pores. Thus, the apparent diffusion coefficient is determined by the diffusion coefficient of the solute in the fluid that fills the pores, the interaction between solute molecules and matrix, the actual length of the diffusion path, and the matrix porosity. For example, the apparent diffusion coefficient of water in cortical bone is two orders of magnitude smaller than the self-diffusion coefficient of water. The ratio of these two values is an indication of the degree of porosity of the matrix and the actual distance traveled by the water molecules, assuming that the interaction between the water molecules and the channel walls does not significantly affect diffusion, which is a sensible assumption for molecules that are small, compared with the pore size [35], [36].

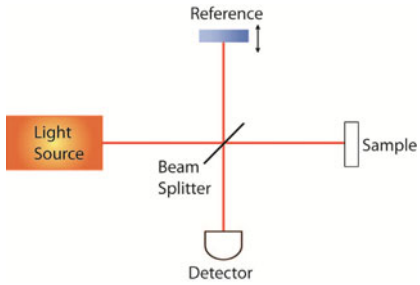

Fig. 1. Simplified diagram of a low-coherence interferometer.

II. *Optical Coherence Tomography*

OCT is an emerging technology that allows producing high-resolution 3-D images of the tissues completely noninvasively and without the need of tissue labeling or application of contrast enhancement agents [37]. The OCT technology was developed on the principles of low-coherence interferometry (LCI) where backscattered photons from a sample of interest are detected within a coherence length of the source using (typically) a two-beam interferometer (see Fig. 1). OCT imaging is somewhat analogous to ultrasound B-mode imaging except that it uses light, not sound. A broadband low-coherence laser source is split equally using a beam splitter into two arms: the reference arm and the sample arm. The back-scattered light from the sample is captured in such a way that it recombines with the light in the reference arm. This recombination results in the formation of fringes, provided the distance traveled by light in both arms should not differ by more than the coherence length of the laser source.

Currently, OCT can be realized in two broad configurations: time domain and Fourier domain. Fig. 2 shows a typical scheme of time-domain OCT. In this configuration, the in-depth scan (typically denoted as z-axis and known as A-scan) is produced by moving the reference mirror. The photodetector receives fringes from matched optical paths in the reference and sample arms that are formed only within coherence length of the source. By moving the reference mirror, the depth profile is formed. By scanning the laser beam across tissue surface (x and y axes) and combining multiple A-scans, 2-D and 3-D cross-sectional images could be formed. Consequently, the acquisition speed of TD-OCT systems is limited by the motion of the reference mirror, which can reach only a few kilohertz speed.

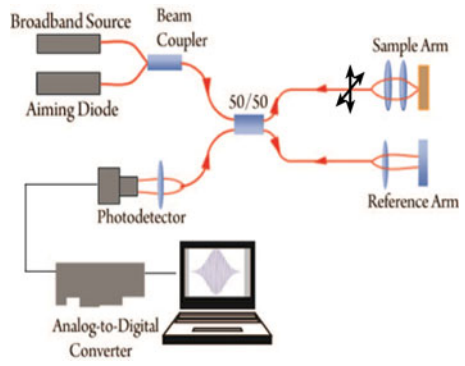

Fig. 2. Time-domain OCT.

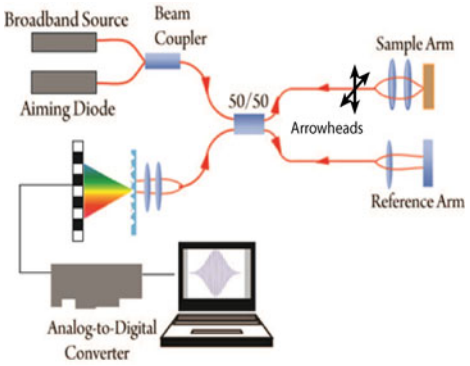

Fig. 3. Spectral-domain OCT.

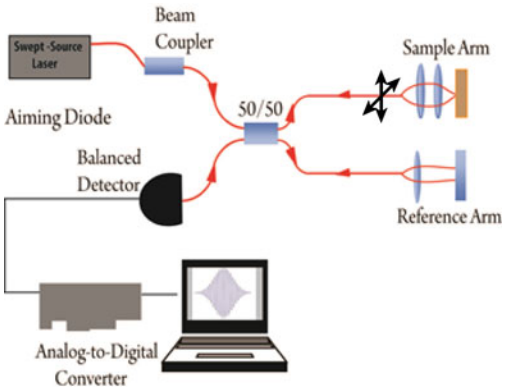

Fig. 4. Swept-source OCT.

Recently, novel OCT detection techniques have emerged which do not require mechanical in-depth scanning and can achieve very high imaging speeds—Fourier-domain OCT (FD-OCT) [38]–[40]. In FD-OCT, the depth information is spectrally encoded that can be extracted by performing Fourier transform of the interference fringes. FD-OCT detection itself can be realized in two configurations of a spectral analysis of the interference signal: 1) spectral-domain OCT (SD-OCT), using a broadband laser source and a spectrometer in the detection arm (see Fig. 3); and 2) swept-source OCT (SS-OCT) using a rapidly tunable, narrow-line-width laser source sweeping over a broad optical bandwidth and a single photodiode in the detection arm (see Fig. 4). Therefore, the speed in FD-OCT is essentially limited by the speed of signal acquisition of the spectrometer (SD-OCT) or sweeping speed of the tunable laser (SS-OCT), which could reach hundreds or, sometimes, even thousands of kilohertz. Moreover, SD-OCT and SS-OCT have significant sensitivity advantages over conventional TDOCT systems of up to 30 dB [38]–[40]. Review of current development and application of OCT technology in many biomedical fields could be found in, e.g., [41]–[45].

III. OCT Imaging Enhancement Using OCAs

OCT provides cross-sectional images of biological tissues over penetration depths of typically 1–3 mm. Although OCT is a unique and useful imaging modality, the relatively shallow penetration depth is considered a serious limitation for many imaging and diagnostic applications. The penetration depth of OCT is fundamentally limited by the attenuation of ballistic light propagation via scattering and absorption. As an OCT beam penetrates deeper into a tissue, the signal strength diminishes. One of the effective techniques to enhance the imaging depth is the application of optical clearing methods that have been shown to be very effective [3], [46]. The application of OCAs, such as glucose or glycerol, on tissue results in local refractive index matching between the intracellular and the extracellular components. As a result, the scattering coefficient of the tissue is reduced permitting the light to reach deeper regions of the tissue. To describe the relationship between the depth of penetration and the signal strength at a particular depth, a method based on OCT signal slope (OCTSS) or OCT amplitude (OCTA) analysis can be used. In the first approximation, the OCTSS plotted on a logarithmic scale is proportional to the total attenuation coefficient of the tissue, μ_t:

$$\ln\left(\frac{I(z)}{I_0}\right) \stackrel{\text{def}}{=} \text{OCTSS} = -\mu_t z = -(\mu_a + \mu_s)z$$

where μ_s and μ_a are the scattering and absorption coefficients, respectively. Since $\mu_s \gg \mu_a$ in the near-infrared (NIR) spectral range

$$\ln\left(\frac{I(z)}{I_0}\right) \stackrel{\text{def}}{=} \text{OCTSS} \approx -\mu_s z.$$

The scattering coefficient of a tissue depends on the refractive index mismatch between the ECF and the tissue components (collagen fibers, cells, etc.). In a simple model of scattering dielectric spheres, μ_s can be approximated as

$$\mu_s = \frac{3.28\pi r^2 \rho_s}{1-g}\left(\frac{2\pi r}{\lambda}\right)^{0.37}\left(\frac{n_s}{n_{\text{ECF}}} - 1\right)^{2.09}$$

where g is the tissue anisotropy factor, r is the radius of scattering centers, ρ_s is the volume density of the scattering centers, λ is the wavelength of the incident light, and n_s and n_{ECF} are the refractive indices of the scattering centers and ECF, respectively [47]. If the refractive index of the scattering centers remains constant and is higher than the refractive index of ECF, the diffusion of molecules inside the medium reduces the refractive index mismatch between n_s and n_{ISF}, and hence, the scattering

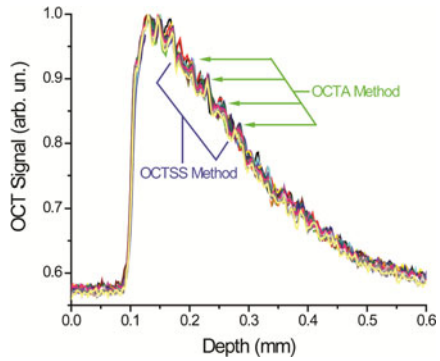

Fig. 5. OCT signals recorded at different times to indicate region and depths for both OCTSS and OCTA analysis methods.

coefficient is also reduced:

$$\mu_s = \frac{3.28\pi r^2 \rho_s}{1-g}\left(\frac{2\pi r}{\lambda}\right)^{0.37}\left(\frac{n_s}{n_{\mathrm{ECF}}+\delta n_{\mathrm{mol}}}-1\right)^{2.09}$$

where δn_{mol} is the molecular-induced increase of the refractive index of ECF. Therefore, an increase in tissue OCA concentration will raise the refractive index of ECF which will decrease the scattering coefficient as a whole.

Alternatively, the change in local concentrations of scattering particles such as cell components or collagen fibers could change scattering as well. Tissues mean refractive index can be calculated by the law of Gladstone and Dale as a weighted average of refractive indices of ECF and collagen fibers or cell components (n_s):

$$\bar{n} = \phi_s n_s + (1-\phi_s) n_{\mathrm{ECF}}$$

where ϕ_s is the volume fraction of collagen fibers and/or cell components in tissues. Therefore, changes in the volume fraction of tissue components (e.g., by shrinkage or swelling of the tissues) will change the overall refractive index of the tissues.

The OCTSS method utilizes the calculation of the average permeability rate *P* of the tissue's layer. The permeability rate can be computed by dividing the thickness of the region used to calculate the OCTSS by the time of molecular permeation in the monitored region $\bar{P} = z_{\mathrm{region}}/t_{\mathrm{region}}$. Prior to the addition of molecules, the baseline signal would remain relatively constant. Only after application, the changes in the OCTSS will be observed. The time interval can be calculated at the time when saturation was achieved (after diffusion) minus the time at which the molecules first reached the region of interest t_{region}. Alternatively, the OCTA method of measurement can be used to calculate the permeability rate at specific depths within the tissue from $P(z) = z_i/t_{zi}$, where z_i is the distance from the surface of the tissue where the measurements are performed and t_{zi} is the time of the agent diffusion to that depth. Fig. 5 shows the representative depiction of the principles for OCTSS and OCTA methods of OCT signal monitoring.

Many studies have been performed on the effect of OCAs on different biological samples. Optical clearing can be estimated by the change in the optical signal obtained from the tissue, after the addition of the clearing agent, as a percentage change. Formally, percentage change at a certain depth of a tissue can be defined as

$$\%\mathrm{clearing} = \frac{(I_2 - I_1)}{I_1} \times 100$$

where I_1 is the optical intensity prior to addition of the clearing agent and I_2 is the optical intensity after the clearing agent has diffused through that particular depth. For example, Ghosn *et al.* showed that 40% of glucose can induce around 10% clearing effect in the upper layer of rabbit sclera, which increases to 22% in the layers below [48]. Larina *et al.* showed how glycerol can be used as a clearing agent which can help better visualize deeper layers in mice embryo [49]. Sudheendran *et al.* monitored the changes in tissue as different concentrations of glucose solution diffused through pig skin [50].

TABLE I
PERMEATION RATES OF VARIOUS DRUGS IN RABBIT CORNEA AND SCLERA

Permeability Rate / Drug	Cornea (cm/sec)	Sclera (cm/sec)
Ciprofloxacin	$(1.85 \pm 0.27) \times 10^{-5}$ (n = 4)	$(1.41 \pm 0.38) \times 10^{-5}$ (n = 3)
Mannitol	$(1.46 \pm 0.08) \times 10^{-5}$ (n = 4)	$(6.18 \pm 1.08) \times 10^{-6}$ (n = 5)
Dexamethasone	$(2.42 \pm 1.03) \times 10^{-5}$ (n = 7)	
Metronidazole	$(1.59 \pm 0.43) \times 10^{-5}$ (n = 5)	$(1.31 \pm 0.29) \times 10^{-5}$ (n = 4)

IV. Quantification of Drug and Molecule Permeation With OCT

OCT capability of 3-D imaging enables precise depth-resolved assessments of optical properties of biological tissues. Previously, it has been demonstrated that the concentration change of OCA in different tissues changes its optical properties [51]–[58]. Most recently, a method that allows for the quantification of the permeation rates of different compounds in tissues using OCTSS has been developed [48], [59]–[67]. Permeation of various molecules and drugs has been quantified in the sclera and the cornea of the eye, monkey skin *in vivo*, and various vascular tissues. Table I shows an example for the permeation rates of various molecules and drugs in the rabbit sclera and cornea measured using OCTSS method described earlier.

Recently, OCT has been also employed to quantify the permeability rates of glucose and different lipoproteins [very low density lipoprotein (VLDL), low-density lipoprotein (LDL), and high-density lipoprotein (HDL)] in vascular tissues (porcine aorta and human carotid endarterectomy (CEA) tissue) [68], [69]. It is also known that structural organization of cells and fibrils composing a tissue could significantly impact the molecular permeability rate and, thus, allowing early detection of tissue abnormalities by quantifying permeability rate in normal versus pathological tissues. For example, the permeability rate of 20% glucose solution in normal vascular tissues was calculated to be $(6.80 \pm 0.18) \times 10^{-6}$ cm/s, while it significantly increased during formation of early arteriosclerotic disease: $(2.69 \pm 0.42) \times 10^{-5}$ cm/s [63].

The influx of lipoproteins is a significant factor in studying the physiological mechanisms that contribute toward the formation of atherosclerosis in vascular tissues. OCT can also be used to measure the perfusion through yet another biological

TABLE II
PERMEATION RATES OF LIPOPROTEINS AND GLUCOSE IN CEA TISSUES AT 20 °C AND 37 °C

	20°C Normal cm/sec	37°C Normal cm/sec	20°C Diseased cm/sec	37°C Diseased cm/sec
VLDL	$(1.13 \pm 0.26) \times 10^{-5}$	$(1.20 \pm 0.25) \times 10^{-5}$	$(1.50 \pm 0.21) \times 10^{-5}$	$(1.75 \pm 0.34) \times 10^{-5}$
LDL	$(3.16 \pm 0.37) \times 10^{-5}$	$(4.77 \pm 0.48) \times 10^{-5}$	$(1.97 \pm 0.34) \times 10^{-5}$	$(2.01 \pm 0.23) \times 10^{-5}$
HDL	$(1.57 \pm 0.26) \times 10^{-5}$	$(2.42 \pm 0.24) \times 10^{-5}$	$(2.01 \pm 0.32) \times 10^{-5}$	$(2.43 \pm 0.31) \times 10^{-5}$
20% Glucose	$(3.51 \pm 0.27) \times 10^{-5}$	$(3.70 \pm 0.44) \times 10^{-5}$	$(6.31 \pm 0.61) \times 10^{-5}$	$(5.70 \pm 0.48) \times 10^{-5}$

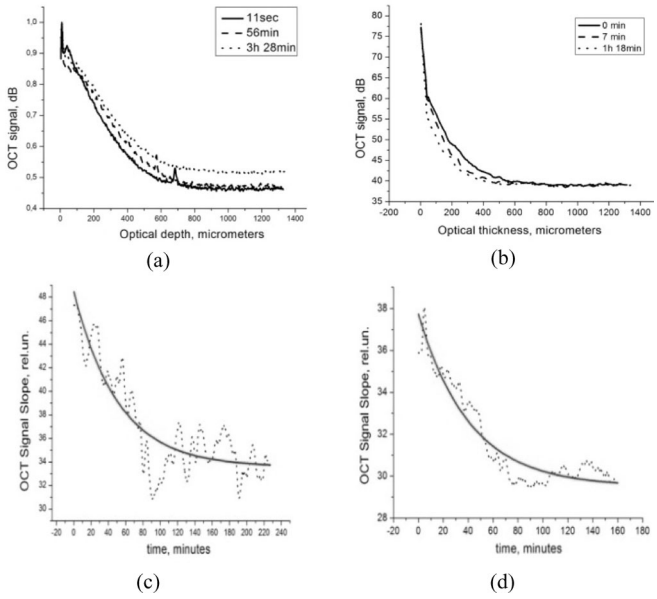

Fig. 6. Example of OCT monitoring of water diffusion in human tooth dentine. *Top*: Averaged A-scans taken at different moments of time for (a) front and (b) back applications. *Bottom*: Mean OCTSS versus time for (c) front and (d) back applications. The probed depth intervals are 150–300 μm for (c) and 60–300 mm for (d).

system, the intimal layer of the carotid arterial wall. This layer is obtained from human CEA specimens, which contain *normal* healthy segments and *diseased* atherosclerotic segments which include lipidic, calcific, hemorrhagic, and/or fibrotic components. The permeation rates of glucose and different lipoproteins were studied at room temperature (20 °C) as well as physiological temperature (37 °C). The results of these permeation studies are summarized in Table II.

Another exciting application of OCT is for diagnostics of disease-caused structural changes in dental tissues [70]–[72]. Monitoring of the molecular diffusion processes was studied in hard tissues such as human tooth and nail as well. Diffusion of water and dental liquor is necessary for teeth functioning and affects the tooth hardness [73]. The permeability of dental tissues is important for dental healing and treatment, cosmetic tooth whitening [74]. The study of water and glycerol application to dentin samples was implemented in two geometries: 1) the sample placed in a cuvette and OCT scanning performed through the liquid layer, covering the sample (front application); 2) the sample glued to a window in the cuvette side face (back application). The sample was coated with hermetic varnish except

TABLE III
TOOTH TISSUE STRUCTURAL AND DIFFUSION PARAMETERS OBTAINED FROM MICROSCOPY AND OCT

Sample number	Sample thickness, $d_{samples}$, mm	Mean tubule diameter, μm	Agent	Time of saturation, min	Permeability Rate, cm/sec
1	0.9	0.60±0.10	water	78	$(3.04\pm0.13)\times10^{-6}$
2	1.3	2.30±0.15	water	9	$(4.02\pm0.24)\times10^{-5}$
3	1.2	1.60±0.13	water	154	$(2.09\pm0.65)\times10^{-6}$
4	0.8	2.4±0.55	44% glycerol solution	54	$(4.91\pm0.67)\times10^{-6}$

a window for OCA diffusion and light penetration in the case of one-side OCA application and two windows on the opposite sides of the sample in the case of backward OCA application. In both cases, OCT scanning was performed repeatedly during a few hours. Fig. 6 shows an example of experimental results for water diffusion in two geometries. The difference between the A-scan behavior for front [see Fig. 6(a)] and backward [see Fig. 6(b)] application may be explained by the competition of the mean attenuation and the back reflectance coefficients. Both are decreased by the diffusing immersion agent, but reduction of the attenuation coefficient leads to OCT signal increase in the sample depth, as the back reflectance decrease causes the corresponding decrease of the OCT signal. A remarkable finding is that in both cases the mean slope of the OCT signal decreases with time and the ultimate damping time constants agree well. Back application is free of artifacts introduced by the liquid layer over the sample and hence was used in further experiments with other agents.

Similar measurements were carried out in other samples with water and 44% glycerol aqueous solution (summarized in Table III). The results demonstrate strong correlation between the diffusion rate and the sample structure, i.e., the tubules diameter and number density. Further studies are expected to quantify this correlation and to construct adequate models allowing for estimation of the tissue optical and diffusion parameters from OCT measurements.

Next, the glucose diffusion and glucose action on the dentin permeability, which is important in the case of *diabetes mellitus*, were studied. Glucose might have a direct effect on the ondoblastic metabolism since it decreases type-I collagen synthesis in mature human odontoblasts *in vitro.* It may also promote the formation of carious lesions. It has been found that the permeability coefficient for 35% aqueous solution of glucose is about two orders of magnitude smaller than that for water (naturally, due to the greater molecule size and, possibly, due to molecular binding). Then, the diffusion process of water in the tooth sample was investigated before and after the long-term glucose action. The sample was kept in 35% aqueous glucose solution for 5 days, and then washed and dried in the same way, as in the measurements with intact samples. The permeability coefficient values of intact and incubated samples were found to be $(2.59 \pm 1.63) \times 10^{-4}$ and $(3.86 \pm 0.39) \times 10^{-4}$ cm/s, respectively. Thus, the long-term glucose impact on the tooth dentin results in irreversible changes of the tissue properties that may result from the glycation-induced change in the intertubular

TABLE IV
SUMMARY OF OCT MEASURED *IN VIVO* ATTENUATION COEFFICIENTS OF FINGERNAIL TISSUE LAYERS FOR THREE SCANNING SITES FOR NORMAL TISSUE μ_t, AT APPLICATION OF GLYCEROL $\mu_{t\mathrm{glyc}}$ AND AT COMPRESSION $\mu_{t\mathrm{compr}}$

Site	μ_t, cm^{-1}			$\mu_{t\,glyc}$, cm^{-1}			$\mu_{t\,compr}$, cm^{-1}		
	Nail	Epid	Der	Nail	Epid	Der	Nail	Epid	Der
I	215.6	32.4	9.8	306.7	17.3	8.1	171.8	18.2	9.8
II	212	20	4.5	256.8	23	-	-	-	-
III	278.1	18	-	264.1	16	-	-	-	-

dentin density and, hence, the increased tubule looseness. Also, an *in vivo* study of molecular diffusion in volunteer's little finger with partly removed nail was performed [75]. OCT measurements allow for identification of each tissue layer and evaluation of its thickness and attenuation (scattering coefficient) if the indices of refraction are known. Taking $n_{\mathrm{nail}} = 1.51$ for nail, $n_{\mathrm{epid}} = 1.43$ for epidermis, and $n_{\mathrm{dermis}} = 1.38$ for dermis, we estimated the attenuation coefficients of fingernail tissue layers for three scanning sites for normal tissue, at application of glycerol and at compression (see Table IV). The effect of glycerol diffusion and pressure is clearly seen in all layers, although the absolute values of the attenuation coefficients differ strongly from the known data obtained by direct attenuation measurements. More efficient algorithms for evaluation of scattering coefficient accounting for multiple scattering should be used to provide quantitative analysis. However, the OCT has proved to be an appropriate technique for comparing the optical properties of a living tissue and a phantom.

Overall, these results demonstrate the capability of OCT technology to quantify time- and depth-dependent diffusion processes in many tissues. Moreover, the difference in diffusion rates between normal and diseased tissues measured with OCT could assist in tissue classification/pathology efforts.

V. *Glucose Sensing With OCT*

Significant effort was devoted to the problem of glucose sensing in biological tissues with OCT. Encouraging results were obtained in several studies for glucose monitoring in animals and human subjects [52], [54], [58]. Hairless Yucatan minipigs and New Zealand white rabbits were used in these studies. The hairless Yucatan minipig is recognized as the best model of human skin [76]. Glucose administrations were performed through the left femoral vein and blood samples were taken from the left femoral artery or right femoral or ear vein. Blood samples were analyzed using standard blood glucose analyzers and compared with OCT readings. Glucose clamping experiments were performed in these animal studies. The clamping technique allowed slow, controlled intravenous administrations of glucose at desired rates to simulate normal physiological changes in blood glucose concentration. Therefore, it minimizes possible tissue physiological responses, such as change in cell volume, ECF fractional volume, and blood microvessel diameter, to sharp increase of the glucose concentration that can be induced by bolus injections.

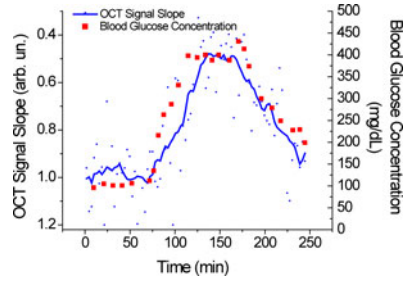

Fig. 7. OCTSS (recorded from minipig skin) and blood glucose concentration measured at different times during glucose clamping experiment [52].

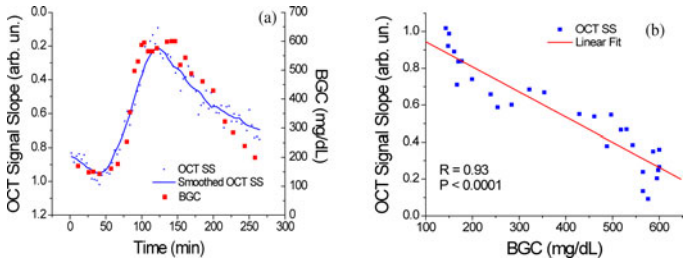

Fig. 8. OCTSS obtained from rabbit lip during (a) glucose clamping experiment versus time and (b) blood glucose concentration [52].

An example of the OCTSS obtained from the Yucatan minipig skin and corresponding blood glucose concentrations measured at different times during the glucose clamping experiment are shown in Fig. 7. Dextrose solution (50% w/w) was administrated for approximately 1 h using a digital pump at a rate of 1.2 mL/min. This resulted in an increase of blood glucose concentration from a baseline level of 100 mg/dL (~5.5 mM) to 400 mg/dL (~22.2 mM). The OCTSS was measured at the depth from 300 to 400 μm and changed approximately 53% in the range from 100 to 400 mg/dL. Good correlation between changes in actual blood glucose concentration and the slope was observed. The lag time between an increase of blood glucose concentration and a decrease of the OCTSS was approximately 14 min. No lag time was observed during subsequent physiological decreases of the blood glucose concentration. Fig. 8(a) shows results obtained from the rabbit lip during a glucose clamping experiment [52]. The blood glucose concentration was increased from 144 to 597 mg/dL starting from the 40th min of the experiment for 80 min. A slow physiological decrease of the blood glucose concentration was monitored for additional 140 min. An eighty percent decrease of the slope of the OCT signal at the depth of 380–480 μm as the blood glucose increased from 144 to 600 mg/dL was observed in this experiment (3.2%/mM). Fig. 8(b) demonstrates good linear correlation between the OCTSS and blood glucose concentration with a correlation coefficient of 0.93 and a p-value less than 0.01.

Typical result obtained from a healthy human volunteer is shown in Fig. 9 [54]. The blood glucose concentration was measured each 15 min during the experiments. Decreases and increases of the OCTSS followed the changes in blood glucose concentration. The slopes changed significantly ~17% with changes in glucose concentration from 90 to 140 mg/dL.

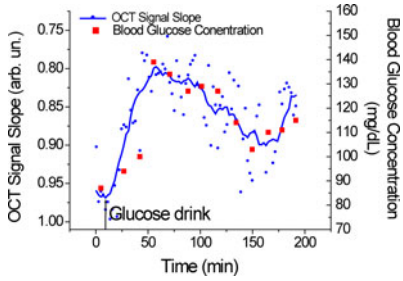

Fig. 9. OCTSS recorded from a human subject and measured blood glucose concentration [54].

These results demonstrated good correlation between changes in slopes of noninvasively measured OCT signals and actual blood glucose concentrations. On average, the slope changed 1.9% per 10 mg/dL change of the blood glucose concentration in these studies. The obtained results were in good agreement with those obtained in animal studies.

VI. Superficial Tissue Inhomogeneities Elimination, Compression Clearing, and Contrasting

The squeezing (compressing) or stretching of a soft tissue causes a significant increase in its optical transmission due to less scattering [11], [77]–[89]. The major mechanisms behind this phenomenon are as follows: 1) increased optical tissue homogeneity due to removal of blood and ECF from the compressed site; 2) more close packing of tissue components leading to constructive interference (cooperative) effects; and 3) less tissue thickness.

Askar'yan [78] was the first to study the propagation of a laser beam through the soft tissue phantoms and human palm at mechanical compression. The reduction of extinction coefficient after tissue compression and prolongation of clearing effect after removing pressure for some time interval was demonstrated.

It should be noted that squeezing-induced effects in tissues containing no or little blood, such as sclera, are characterized by a marked inertia (a few minutes) because of the relatively slow diffusion of water from the compressed region [11], [85]. It was proposed that compression of sclera may displace water from the interspace of collagen fibrils, increasing the protein and mucopolysaccharide concentrations. Since these proteins and sugars have refractive index closer to that of the collagen fibrils, a more index-matched environment can be created. On the other hand, compression reduces specimen thickness d, which might increase the effective scatterer concentration inside the tissue. Therefore, compression may also give rise to an increase in tissue scattering coefficient μ_s. Sometimes, the increase in scatterer concentration is likely to be more dominant than the reduction in index mismatch [89]. In addition, reduction of tissue thickness causes an increase in local chromophore concentration; thus, the absorption coefficient μ_a increases. However, the total effect on optical properties change, which is proportional to the product of $(\mu_s + \mu_a)d$, is characterized by a less light attenuation, due to much less thickness of compressed soft tissue (up to 72%) [86], [87], [89]; cooperative effects also may have a great influence in reduction of the overall scattering [11].

As a well-blood-supplied tissue, skin spectral properties can be effectively controlled by applying an external localized pressure in *in vivo* experiments when UV-induced erythema (skin redness) is developed [88]. For that particular case, extra blood in the skin dermis coming due to physiological reaction on UV light is pushed out by compression, thus providing better light transmittance within the bands of Hb even the erythema without compression is rather strong.

Steady-state diffuse reflectometry with a variable source–detector separation $r_{\rm sd}$ allows one to characterize properties of light propagation in a tissue at mechanical tension, including its anisotropy followed the stretching direction [84]. At external forced tension, more significant damping of scattering along the direction of mechanical stress is expected.

The estimation of biomechanical properties of tissue is critical to many areas of the health sciences, including monitoring of the tension in wound closures, skin flaps, and tissue expanders. *In vivo* human experiments showed that the specular reflection from skin changes with stretch [81]. For small values of skin stretch, the specular reflectivity measured for the He:Ne laser ($\lambda = 633$ nm) beam with the 45° angle of incidence increases linearly with strain showing considerable anisotropic properties [81].

All aforementioned early studies of tissue compression have stimulated application of this technology to OCT, where the penetration depth and image contrast issues are critical. A hemispherically tipped glass rod (borosilicate, $n_{\rm glass} = 1.474$) 20 mm long with a 3-mm tip diameter was used as a probe for localized skin compression and concurrent OCT imaging at a mean wavelength of 1310 nm (swept source OCT system) [80]. The glass rod did not add any perceivable distortions to the OCT signal. The stepwise loading protocol allowing for removal of the transient viscoelastic response of the tissue, thus capturing the quasi-static mechanical deformation response, was used for *ex vivo* and *in vivo* skin imaging. To measure changes in skin thickness and refractive index due to compression, OCT images were obtained at each indentation step. The authors of [80] have demonstrated that for similar effective tissue strain, air dehydration and mechanical compression produce similar changes in refractive index and water volume fraction. These data directly proof the concept that mechanical compression may cause local water removal within compressed regions of the tissue. This water may then be transported laterally along interstitial pressure gradients, increasing local protein concentration. Mechanical compression results in higher OCT signal intensity, i.e., higher contrast and thus better imaging capability. The localized mechanical compression of skin decreases tissue thickness and water content and increases refractive index and OCT signal intensity. Mechanical loading may also decrease absorption and scattering in the compressed region, particularly at 1310 nm, near the 1450 nm absorption peak of water (low concentration of water due to its displacement).

The effect of mechanical compression in contrast between epithelial and stromal layers of human rectum *ex vivo* in OCT images was studied in [77]. Due to different mechanical properties and water content of these layers, the changes in scattering properties induced by compression are different, which leads

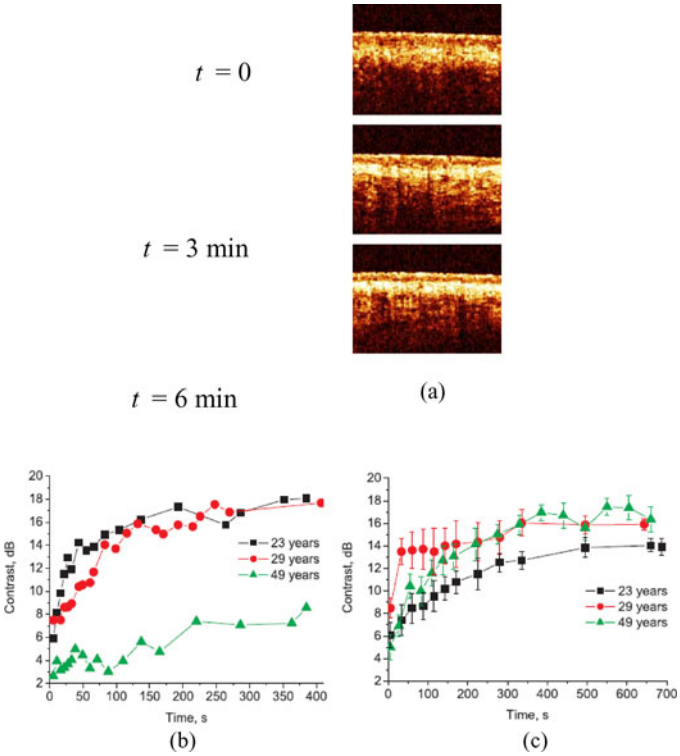

Fig. 10. (a) OCT images of thin skin of the 29-year-old male volunteer immediately after compression started ($t = 0$), in 3 min, and in 6 min for high-pressure regime (0.35 N/mm^2); (b) and (c) temporal characteristics of contrast of the epidermis–dermis junction for three volunteers of different ages for low-pressure (0.07 N/mm^2) and high-pressure (0.35 N/mm^2) compression [83].

to better contrasting of these layers in OCT images. The same group has reported recently studies on continuous mechanical compression of human thin skin *in vivo* [83]. The OCT images were obtained for three male volunteers of different ages at low and high mechanical pressures. The OCT probe was placed in a special holder allowing for control of the force of pressure on the skin and keeping it constant. The probe was pressed onto human skin with the force varying from 0.4 N (pressure 0.07 N/mm^2) to 2 N (0.35 N/mm^2) and was held in such a position for 10–15 min while the OCT images of the skin were acquired continuously at a rate of 1 image every 5 s. The force was controlled by a specially designed OCT probe holder with a dynamometer. To characterize the effect of mechanical compression on the optical properties of skin layers, an image contrast was introduced: the OCT signal (A-scan) was averaged over the transverse direction in the region uniform in the transverse (in respect to the probe beam) direction of 200 μm width [see Fig. 10(a)]; from this averaged A-scan OCT signals (in dB) for particular layers were extracted; the difference of these signals for neighboring layers was attributed as image contrast corresponding to the ratio of the OCT signals indicated in dB [see Fig. 10(b) and (c)]. The temporal dependences of OCT image contrast for the epidermis–dermis junction measured at low and high pressures are presented in Fig. 10(b) and (c). For the 23-year-old volunteer, the image contrast increased monotonically with time for both the low- and high-pressure regimes. For the 29-year-old volunteer, the maximal contrast was reached much faster for the high pressure than for the lower, less than 1 min was enough to reach the similar contrast for which at the low pressure more than 3 min was needed. The skin of the older volunteer (49 years old) demonstrates an increase in junction contrast especially at the high-pressure regime that reaches similar maximum as for younger skin at the sixth min. Evidently, these changes could be associated with different dynamics of water inflow, in particular connected with the different balance of free and bounded water for the young and aged skin and different elasticity of the skin of the various age groups [83]. It is well known that skin water content decreases with age since the amount of glycosaminoglycans declines with age, as does the amount of hyaluronic acid produced by fibroblasts and the amount of interfibrillary ground substance [90]. Since change in epidermal thickness under pressure does not correlate with the age of the volunteers, the observed increase of the measured OCT image contrast deals with changing the skin dermis scattering properties [83]. The compression induces increasing skin scattering coefficient [89] and corresponding decreasing OCT signal [3]. At low pressure [see Fig. 10(b)], water inflow from the water-filled dermis of young volunteers is more expressed in contrast to that of an older volunteer as a result of smaller hydration of the aged skin dermis and more rigidity of the dermis due to loss of the hyaluronic acid production. However, in the case of high pressure the dermis of an old volunteer has more significant deformation and so the measured contrast increases similar to the young skin.

VII. Monitoring of Skin Perforation and Nanoparticle Delivery

Several promising diagnostic and therapeutic technologies rely on micro- and nanoparticles delivery into a tissue and use them as contrasting agents or mediators of laser heating [2]. Multiple studies are devoted to the transportation of nanoparticles in cells and various biological tissues. An important problem is the understanding how nanoparticles are distributed in the tissues. For example, titanium dioxide, zinc oxide, and gold nanoparticles are used as contrasting agents for OCT imaging of skin [91], [92]. Nanoparticles can also serve as carriers of drugs, mRNAs, and other therapeutic formulations upon their transcutaneous administration [93]. For example, gold nanoparticles are used for photothermal treatment of neoplasms hidden inside a tissue layer [94], [95]. In [96] for the TiO_2 and Ag–SiO_2 nanoparticles, a phototoxic action on pathogenic microorganisms was demonstrated caused by both the nanoparticles themselves and their combination with dyes.

The main advantage of transcutaneous administration of the formulations (including nanoparticles) is that the delivery is targeted directly to the pathologically modified areas of the tissue [97]. Creation of artificial channels by means of microporation helps to overcome the protective skin barrier and promotes deeper and more targeted delivery of nanoparticles [97]. In this case, the diameter and the depth of pores depend on the instruments, acting on the skin.

Several studies have demonstrated that OCT can be an effective method for monitoring of nanoparticle delivery into skin [91], [92]. The method is based on the high refractive index

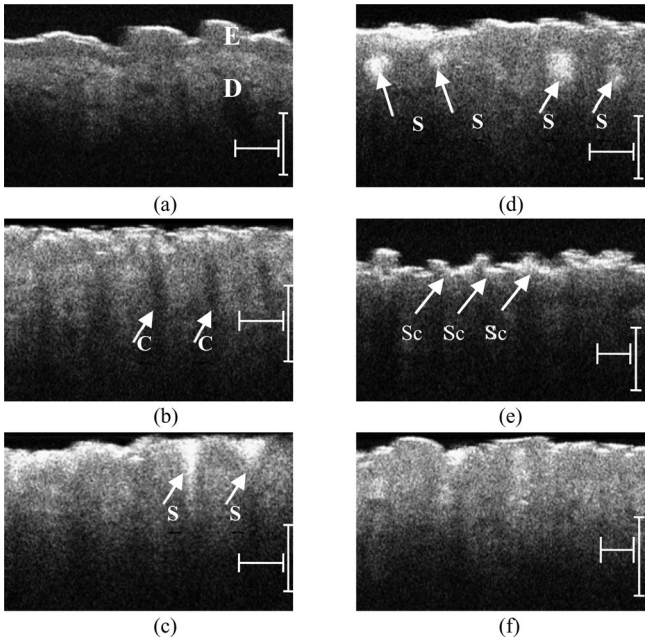

Fig. 11. OCT images of the human skin *in vivo*: (a) intact skin; (b) skin after microablation by a laser pulse; (c) skin after 2 h; (d) skin after 24 h; (e) skin after 6 days; and (f) skin after 2 weeks after TiO_2 nanoparticles administration. E denotes the epidermis, D the dermis, C the microchannels, S the TiO_2 suspension, and Sc the scab with TiO_2 nanoparticles. Arrows point at the areas of ablation. Bars correspond to 500 μm.

mismatching between biological tissues and metal nanoparticles that causes the high contrast level of nanoparticle imaging in the tissue. As an example, Fig. 11 presents the OCT images of the forearm skin before the microporation and after the fractional laser microablation and insertion of nanoparticles. The Palomar Lux2940 erbium laser (Palomar Medical Products Ltd., MA) was used as a light source. Its parameters were as follows: the wavelength of 2940 nm, the pulse energy of 3.0 J, and the pulse duration of 20 ms. The microchannels were produced by means of an attachment that allowed for microablation channels of skin areas. Suspension of TiO_2 nanopowder (Sigma-Aldrich Co., MO) with the nanoparticle size less than 100 nm in PEG with the MW 300 (Sigma-Aldrich Co., USA) was used. The concentration of nanoparticles in the suspension was 0.5 g/mL. The treated area was massaged for 5 min, and then covered by polyethylene film and bandaged in 2 h. Then, the particles were removed by distilled water. The observations were carried out over a month period. Fig. 11(a) shows the OCT scan of the intact skin region. The depth of probing is about 500 μm. A papillary structure of epidermis on the surface of the skin and a boundary between epidermis and dermis are clearly visible. In Fig. 11(b), the arrows indicate ablation channels just after the microporation. The depth of microchannels was about 500 μm. The next imaging was obtained just after the removal of the suspension from the skin surface. In this figure, the microchannels filled by TiO_2 suspension are clearly seen (marked with arrows). The depth of penetration of nanoparticles coincides with that of the microscopic channels. In 24 h, it has become evident that the microchannels are filled with the suspension in depth, but near the surface nanoparticles are absent [see Fig. 11(d)]. In Fig. 11(e), which corresponds 6-day posttreatment, we can see the complete healing of microchannels and particular disappearing of nanoparticles from the skin. The peeling of the damaged surface layer of epidermis also begins at this point. On the skin surface, a scab containing nanoparticles (marked with arrows) forms a solid layer, which simulates a reflecting screen. Therefore, the probing depth decreases up to about 200 μm in the area of the microchannels. Two weeks after the experiment, the peeling finished and the integrity of the epidermis was restored [see Fig. 11(f)]. It is clear that the skin surface becomes smoother in comparison with initial state [see Fig. 11(a)]. A possible increase in light scattering may be explained by the presence of some part of nanoparticles that do not leave the skin as a result of the natural motion together with the epidermis cells toward the surface in the course of the cell division. After the restoration of the skin integrity, the nanoparticles, inserted at the depth exceeding the epidermis thickness (100–150 μm), stay in the dermis, providing amplified scattering.

Nanoparticle application is also of great interest for the reduction of the tooth sensitivity, restoration and strengthening of enamel, and cosmetic whitening. The problems and prospects of using nanoparticles and nanotechnologies in stomatology are summarized in recent review [98]. To close the dentine tubules and thus to reduce the tooth sensitivity, laser ablation of gold nanoparticles was used [99]. The efficiency of antibacterial nanoparticles delivery providing the disinfection of the root channel was increased using high-intensity ultrasound, causing the collapse of cavitation bubbles [100]. Aimed at dentin whitening, the authors of [101] used 3.5% solution of hydrogen peroxide with suspension of titanium dioxide nanoparticles (TiO_2), applied to the dentin sections with subsequent illumination with the diode laser at 405 nm or with a halogen lamp. Spectrophotometric measurements demonstrated significant whitening effect as a result of this combined action. In [102], the restoration of the tooth enamel using the hydroxyapatite nanoparticles was investigated and the role of the particle size was demonstrated.

Using OCT, the penetration of TiO_2 nanoparticles (size $<$ 100 nm, Aldrich, MO) from a suspension in Poly(sodium4-styrene-sulfonate) with the concentration of 10 mg/mL into the tooth dentin and enamel samples was studied. After the OCT scanning of intact samples, they were merged into the cuvette with the suspension of TiO_2 nanoparticles and placed into an ultrasonic bath for 15 min to stimulate the nanoparticle penetration into the tooth tissue. The sample was washed with water and dried in the air flow for 30 min to remove the remainders of the suspension from the surface and the OCT scanning was carried out. Such a procedure was repeated several times, after which the samples were again merged into the cuvette with TiO_2 suspension and kept to the next day. The total time of the experiment with one sample was 10 days.

Fig. 12 shows that the profile of A-scan changes with time, and the greatest increase of the signal (up to 5 dB) is observed directly under the surface and at the depths of 300–600 μm from the surface of the sample. This may be attributed to the penetration of TiO_2 nanoparticles into the dentin and enamel. However, it is hard to determine the penetration depth more

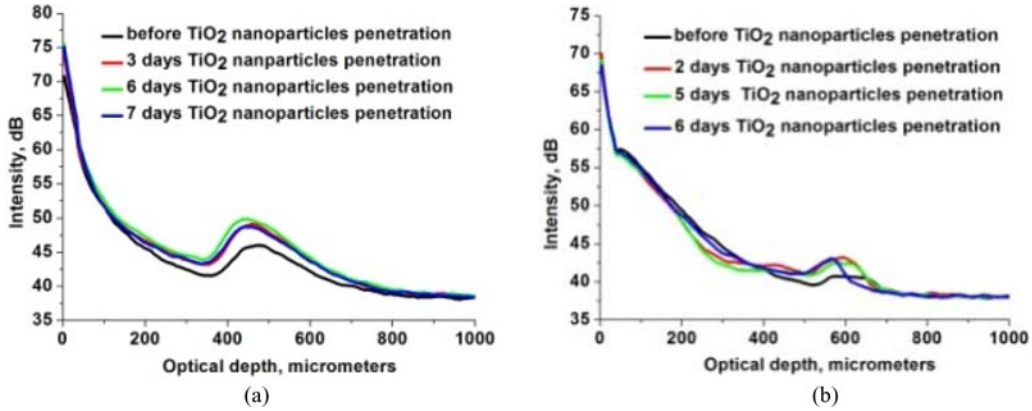

Fig. 12. Averaged A-scans at different moments of time in the course of treatment of (a) dentine and (b) enamel with the suspension of TiO_2 nanoparticles.

precisely, because the nanoparticles in the near-surface region can significantly increase the contribution of multiply scattered photons with greater delay times. Being interpreted in terms of a single-scattering model, this effect will be seen as nanoparticle penetration at greater depth. The peak at 400–600 μm is an image of the backside of the thin sample, blurred by multiple scattering. The diffusion of the solvent should cause optical clearing, which appears to be smaller than the increase of scattering due to the introduced nanoparticles.

VIII. Conclusion Remarks: Safety and Toxicity Issues

Here, we reviewed OCT technology in application of assessment of molecular and nanoparticle diffusion in different tissues. Widely used hyperosmotic fluids (e.g., glucose, glycerol, mannitol, and propylene glycol) are generally nontoxic agents. However, they can induce cell apoptosis, local hemostasis, and even tissue necrosis, with prolonged application of highly concentrated OCAs, due to the induction of osmotic stress [103], [104].

The *in vivo* effect of anhydrous glycerol on cutaneous vasculature has been studied by Doppler OCT [56]. An important finding of that study was that the effect of glycerol on vessels was reversible with rehydration; when the skin was rehydrated using saline applied to the skin site, flow in arterioles and venules returned to physiologic values and remained at those values.

The study of kinetics of optical clearing of rat skin *in vivo* at 84.4% glycerol intradermal injection has shown transition from the oxygenated form of Hb to the deoxygenated form 15 min after injection [105]. It was suggested that this effect was related to local hemostasis of skin vessels caused by the high concentration of glycerol.

Long-term effects on blood vessels were investigated by observing the function and the development of blood vessels in chick chorioallantoic membrane. The results have shown that in 2 days after glycerol application, the blood flow velocity was recovered to different extents, and new blood vessels were developed nearby. Glucose induced slow changes in blood flow. However, most blood vessels were blocked and no new blood vessels developed in 2 days [106].

Membrane-impermeable sugar alcohols, such as mannitol, glycerol, etc., decrease cell volume due to the increase of the osmolarity of the medium and induce osmotic water loss. This effect can induce cell apoptosis [104]. Volume changes (shrinkage and swelling) are also observed in fibrous tissues. They are induced by osmotic dehydration of tissue, differences in pH of ECF and OCAs, as well as hygroscopic property of the agents, which can bond water molecules in the extracellular space [12], [13].

The irreversible changes of collagen structure under the action of pure glycerol are also possible [14]. However, this effect is observed in tendon and model samples that have well-ordered fibrillar organization. After glycerol removal and rehydration of the samples, the structure does not reshape totally. In softer skin, this effect can be reversible [14]. *In vivo* experiments have shown that the glycerol solution of 75% does not induce any loss of collagen organization [13].

Studies on wear debris particles from surgical implants and other toxicity studies on insoluble particles support the traditional toxicology view that the hazard of small particles is mainly defined by the intrinsic toxicity of particles, as distinct from their particle size. Many groups have investigated the cellular toxicity of nanoparticles with regard to particle size, shape, and surface group [90]–[95]. Toxicity can be positive as well as negative property of nanoparticles in dependence on the goals of application. If nanoparticles are used as contrast agents for improvement of tissue visualization, they must be nontoxic. For photodynamic application, on the contrary, cytotoxity of nanoparticles is very important. Nevertheless, cytotoxicity, genotoxicity, and photogenotoxicity studies on insoluble nanoparticles should be interpreted with caution, since such toxicities may be secondary to phagocytosis of mammalian cells exposed to high concentrations of insoluble particles [107].

The results of exposure of the human leukemia cells to the spherical nanoparticles were toxic to the cells up to $\sim$100 μM in gold concentration, even though they were being taken up into the cells [108], [109]. Similar viability studies with immune system cells also showed that gold nanoparticles were not cytotoxic and that they reduced the amount of potentially harmful reactive oxygen species in the cells [109]. However, it was observed that surface modifier as a cetyltrimethylammonium bromide (CTAB), which may result from incomplete purification of the gold nanorods or desorption from the bound bilayer, can be toxic to cells, because it is a detergent that can

break open cell membranes [110], [111]. This toxicity of CTAB can be reduced by overcoating the nanorods with PEG, which is a well-known procedure to overcome nonspecific binding of biological molecules to surfaces [111]. Phosphatidylcholine is another biocompatible overcoating molecule that reduces the reported cytotoxicity of CTAB-coated gold nanorods [112].

Zinc oxide and titanium dioxide nanoparticles (20–30 nm) are widely used in several topical skin care products, such as sunscreens. Overall, the current weight of evidence suggests that nanomaterials such as nanosized vesicles or ZnO and TiO_2 nanoparticles currently used in cosmetic preparations or sunscreens pose no risk to human skin or human health, although other nanoparticles may have properties that warrant safety evaluation on a case-by-case basis before human use [107].

ACKNOWLEDGMENT

The authors would like to thank Prof. V. L. Derbov for his help in preparation of this paper.

REFERENCES

[1] V. V. Tuchin, "Optical clearing of tissues and blood using the immersion method," *J. Phys. D, Appl. Phys.*, vol. 38, pp. 2497–2518, Aug. 2005.

[2] E. A. Genina, A. N. Bashkatov, and V. V. Tuchin, "Tissue optical immersion clearing," *Expert Rev. Med. Devices*, vol. 7, pp. 825–842, Nov. 2010.

[3] V. V. Tuchin, *Tissue Optics: Light Scattering Methods and Instruments for Medical Diagnosis*, 2nd ed. Bellingham, WA: SPIE, 2007.

[4] J. M. Schmitt and G. Kumar, "Optical scattering properties of soft tissue: A discrete particle model," *Appl. Opt.*, vol. 37, pp. 2788–2797, May 1998.

[5] K. Sokolov, R. Drezek, K. Gossage, and R. Richards-Kortum, "Reflectance spectroscopy with polarized light: Is it sensitive to cellular and nuclear morphology," *Opt. Exp.*, vol. 5, pp. 302–317, Dec. 1999.

[6] D. W. Leonard and K. M. Meek, "Refractive indices of the collagen fibrils and extrafibrillar material of the corneal stroma," *Biophys J.*, vol. 72, pp. 1382–1387, Mar. 1997.

[7] A. N. Yaroslavsky, A. V. Priezzhev, J. Rodriguez, I. V. Yaroslavsky, and H. Battarbee, "Optics of blood," in *Handbook of Optical Biomedical Diagnostics*, V. V. Tuchin, Ed. Bellingham, WA: SPIE Press, 2002, pp. 169–216.

[8] G. Mazarevica, T. Freivalds, and A. Jurka, "Properties of erythrocyte light refraction in diabetic patients," *J. Biomed. Opt.*, vol. 7, pp. 244–247, Apr. 2002.

[9] M. Friebel and M. Meinke, "Model function to calculate the refractive index of native hemoglobin in the wavelength range of 250–1100 nm dependent on concentration," *Appl. Opt.*, vol. 45, pp. 2838–2842, Apr. 2006.

[10] O. Zhernovaya, O. Sydoruk, V. Tuchin, and A. Douplik, "The refractive index of human hemoglobin in the visible range," *Phys. Med. Biol.*, vol. 56, pp. 4013–4021, Jul. 2011.

[11] V. V. Tuchin, *Optical Clearing of Tissues and Blood*, vol. PM 154. Bellingham, WA: SPIE Press, 2006.

[12] A. N. Bashkatov, E. A. Genina, Y. P. Sinichkin, V. I. Kochubey, N. A. Lakodina, and V. V. Tuchin, "Glucose and mannitol diffusion in human dura mater," *Biophys J.*, vol. 85, pp. 3310–3318, Nov. 2003.

[13] X. Wen, Z. Mao, Z. Han, V. V. Tuchin, and D. Zhu, "In vivo skin optical clearing by glycerol solutions: Mechanism," *J. Biophotonics*, vol. 3, pp. 44–52, Jan. 2010.

[14] A. T. Yeh, B. Choi, J. S. Nelson, and B. J. Tromberg, "Reversible dissociation of collagen in tissues," *J. Invest. Dermatol.*, vol. 121, pp. 1332–1335, Dec. 2003.

[15] E. Genina, A. Bashkatov, and V. V. Tuchin, "Optical clearing of cranial bone," *Adv. Opt. Technol.*, vol. 2008, art ID 267867, 8 pp., 2008.

[16] A. Roggan, M. Friebel, K. Dorschel, A. Hahn, and G. Muller, "Optical properties of circulating human blood in the wavelength range 400–2500 nm," *J. Biomed. Opt.*, vol. 4(1), pp. 36–46, 1999.

[17] V. V. Tuchin, X. Xu, and R. K. Wang, "Dynamic optical coherence tomography in studies of optical clearing, sedimentation, and aggregation of immersed blood," *Appl. Opt.*, vol. 41, pp. 258–271, Jan. 2002.

[18] V. Tuchin, D. Zhestkov, A. Bashkatov, and E. Genina, "Theoretical study of immersion optical clearing of blood in vessels at local hemolysis," *Opt. Exp.*, vol. 12, pp. 2966–2971, Jun. 2004.

[19] G. Popescu, T. Ikeda, C. A. Best, K. Badizadegan, R. R. Dasari, and M. S. Feld, "Erythrocyte structure and dynamics quantified by Hilbert phase microscopy," *J. Biomed. Opt.*, vol. 10, 060503, Nov./Dec. 2005.

[20] H. Schaefer and T. E. Redelmeier, *Skin Barrier*. Basel, Switzerland: Karger, 1996.

[21] J. Hadgraft, "Skin, the final frontier," *Int. J. Pharm.*, vol. 224, pp. 1–18, Aug. 2001.

[22] R. H. Guy and J. Hadgraft, "Physicochemical aspects of percutaneous penetration and its enhancement," *Pharm. Res.*, vol. 5, pp. 753–758, Dec. 1988.

[23] R. H. Guy and J. Hadgraft, "Percutaneous penetration enhancement: Physicochemical considerations and implications for prodrug design," *Clin. Res. Reg. Affairs*, vol. 18, pp. 219–233, 2001.

[24] S. A. Ibrahim and S. K. Li, "Effects of chemical enhancers on human epidermal membrane: Structure-enhancement relationship based on maximum enhancement (E(max))," *J. Pharm. Sci.*, vol. 98, pp. 926–944, Mar. 2009.

[25] K. Kretsos, M. A. Miller, G. Zamora-Estrada, and G. B. Kasting, "Partitioning, diffusivity and clearance of skin permeants in mammalian dermis," *Int. J. Pharm.*, vol. 346, pp. 64–79, Jan. 2008.

[26] S. Mitragotri, "In situ determination of partition and diffusion coefficients in the lipid bilayers of stratum corneum," *Pharm. Res.*, vol. 17, pp. 1026–1029, Aug. 2000.

[27] A. Edwards and M. R. Prausnitz, "Fiber matrix model of sclera and corneal stroma for drug delivery to the eye," *AIChE J.*, vol. 44, pp. 214–225, 1998.

[28] K. D. Peck, A. H. Ghanem, and W. I. Higuchi, "Hindered diffusion of polar molecules through and effective pore radii estimates of intact and ethanol treated human epidermal membrane," *Pharm. Res.*, vol. 11, pp. 1306–1314, Sep. 1994.

[29] W. M. Deen, "Hindered transport of large molecules in liquid-filled pores," *AIChE J.*, vol. 33, pp. 1409–1425, 1987.

[30] O. A. Boubriak, J. P. Urban, and A. J. Bron, "Differential effects of aging on transport properties of anterior and posterior human sclera," *Exp. Eye. Res.*, vol. 76, pp. 701–713, Jun. 2003.

[31] D. M. Maurice, "The regurgitation of large vitreous injections," *J. Ocul. Pharmacol. Ther.*, vol. 13, pp. 461–463, Oct. 1997.

[32] M. R. Prausnitz and J. S. Noonan, "Permeability of cornea, sclera, and conjunctiva: A literature analysis for drug delivery to the eye," *J. Pharm. Sci.*, vol. 87, pp. 1479–1488, Dec. 1998.

[33] K. H. Mueller, A. Trias, and R. D. Ray, "Bone density and composition. Age-related and pathological changes in water and mineral content," *J. Bone Joint Surg. Amer.*, vol. 48, pp. 140–148, Jan. 1966.

[34] S. R. Elliott and R. A. Robinson, "The water content of bone: I. The mass of water, inorganic crystals, organic matrix, and CO_2 space components in a unit volume of the dog bone," *J. Bone Joint Surg. Amer.*, vol. 39-A, pp. 167–188, Jan. 1957.

[35] M. A. Fernandez-Seara, S. L. Wehrli, and F. W. Wehrli, "Diffusion of exchangeable water in cortical bone studied by nuclear magnetic resonance," *Biophys J.*, vol. 82, pp. 522–529, Jan. 2002.

[36] A. Maroudas, "Distribution and diffusion of solutes in articular cartilage," *Biophys J.*, vol. 10, pp. 365–379, May 1970.

[37] D. Huang, E. A. Swanson, C. P. Lin, J. S. Schuman, W. G. Stinson, W. Chang, M. R. Hee, T. Flotte, K. Gregory, C. A. Puliafito, and J. G. Fujimoto, "Optical coherence tomography," *Science*, vol. 254(5035), pp. 1178–1181, 1991.

[38] M. A. Choma, M. V. Sarunic, C. H. Yang, and J. A. Izatt, "Sensitivity advantage of swept source and Fourier domain optical coherence tomography," *Opt. Exp.*, vol. 11, pp. 2183–2189, 2003.

[39] J. F. de Boer, B. Cense, B. H. Park, M. C. Pierce, G. J. Tearney, and B. E. Bouma, "Improved signal-to-noise ratio in spectral-domain compared with time-domain optical coherence tomography," *Opt. Lett.*, vol. 28, pp. 2067–2069, 2003.

[40] R. Leitgeb, C. K. Hitzenberger, and A. F. Fercher, "Performance of Fourier domain versus time domain optical coherence tomography," *Opt. Exp.*, vol. 11, pp. 889–894, 2003.

[41] S. Marschall, B. Sander, M. Mogensen, T. M. Jørgensen, and P. E. Andersen, "Optical coherence tomography—Current technology and applications in clinical and biomedical research," *Anal. Bioanal. Chem.*, vol. 400, pp. 2699–2720, 2011.

[42] M. L. Gabriele, G. Wollstein, H. Ishikawa, L. Kagemann, J. Xu, L. S. Folio, and J. S. Schuman, "Optical coherence tomography: History, current status, and laboratory work," *Investigative Ophthalmology Visual Sci.*, vol. 52, pp. 2425–2436, Apr. 2011.

[43] M. Wojtkowski, "High-speed optical coherence tomography: Basics and applications," *Appl. Opt.*, vol. 49, pp. D30–D61, Jun. 2010.
[44] M. E. Brezinski, *Optical Coherence Tomography: Principles and Applications*. Amsterdam, The Netherlands: Academic, 2006.
[45] W. Drexler and J. G. Fujimoto, *Optical Coherence Tomography: Technology and Applications*. Berlin, Germany: Springer, 2008.
[46] V. V. Tuchin, *Handbook of Photonics for Biomedical Science*. Boca Raton, FL: CRC Press, 2010.
[47] R. Graaff, J. G. Aarnoudse, J. R. Zijp, P. M. A. Sloot, F. F. M. Demul, J. Greve, and M. H. Koelink, "Reduced light-scattering properties for mixtures of spherical-particles—A simple approximation derived from Mie calculations," *Appl. Opt.*, vol. 31, pp. 1370–1376, Apr. 1992.
[48] M. G. Ghosn, E. F. Carbajal, N. Befrui, V. V. Tuchin, and K. V. Larin, "Differential permeability rate and percent clearing of glucose in different regions in rabbit sclera," *J. Biomed. Opt.*, vol. 13, 021110, 2008.
[49] I. V. Larina, E. F. Carbajal, V. V. Tuchin, M. E. Dickinson, and K. V. Larin, "Enhanced OCT imaging of embryonic tissue with optical clearing," *Laser Phys. Lett.*, vol. 5, pp. 476–480, 2008.
[50] N. Sudheendran, M. Mohamed, M. Ghosn, V. V. Tuchin, and K. V. Larin, "Assessment of tissue optical clearing as a function of glucose concentration using optical coherence tomography," *J. Innovative Opt. Health Sci.*, vol. 3, pp. 169–176, 2010.
[51] K. V. Larin, T. Akkin, R. O. Esenaliev, M. Motamedi, and T. E. Milner, "Phase-sensitive optical low-coherence reflectometry for the detection of analyte concentrations," *Appl. Opt.*, vol. 43, pp. 3408–3414, 2004.
[52] K. V. Larin, M. Motamedi, T. V. Ashitkov, and R. O. Esenaliev, "Specificity of noninvasive blood glucose sensing using optical coherence tomography technique: A pilot study," *Phys. Med. Biol.*, vol. 48, pp. 1371–1390, 2003.
[53] A. I. Kholodnykh, I. Y. Petrova, K. V. Larin, M. Motamedi, and R. O. Esenaliev, "Precision of measurement of tissue optical properties with optical coherence tomography," *Appl. Opt.*, vol. 42, pp. 3027–3037, 2003.
[54] K. V. Larin, M. S. Eledrisi, M. Motamedi, and R. O. Esenaliev, "Noninvasive blood glucose monitoring with optical coherence tomography—A pilot study in human subjects," *Diabetes Care*, vol. 25, pp. 2263–2267, 2002.
[55] G. Vargas, K. F. Chan, S. L. Thomsen, and A. J. Welch, "Use of osmotically active agents to alter optical properties of tissue: Effects on the detected fluorescence signal measured through skin," *Lasers Surg. Med.*, vol. 29, pp. 213–220, 2001.
[56] G. Vargas, A. Readinger, S. S. Dozier, and A. J. Welch, "Morphological changes in blood vessels produced by hyperosmotic agents and measured by optical coherence tomography," *Photochem. Photobiol.*, vol. 77, pp. 541–549, May 2003.
[57] A. T. Yeh and J. Hirshburg, "Molecular interactions of exogenous chemical agents with collagen—Implications for tissue optical clearing," *J. Biomed. Opt.*, vol. 11(1), 014003, 2006.
[58] R. O. Esenaliev, K. V. Larin, I. V. Larina, and M. Motamedi, "Noninvasive monitoring of glucose concentration with optical coherence tomography," *Opt. Lett.*, vol. 26, pp. 992–994, Jul. 2001.
[59] E. A. Genina, A. N. Bashkatov, V. V. Tuchin, M. Ghosn, K. V. Larin, and T. G. Kamenskikh, "Cortexin diffusion in human eye sclera," *Quantum Electron.*, vol. 41, pp. 407–413, 2011.
[60] M. Ghosn, N. Sudheendran, M. Wendt, A. Glasser, V. V. Tuchin, and K. V. Larin, "Monitoring of glucose permeability in monkey skin in vivo using optical coherence tomography," *J. Biophotonics*, vol. 3, pp. 25–33, 2010.
[61] M. G. Ghosn, S. H. Syed, N. A. Befrui, M. Leba, A. Vijayananda, N. Sudheendran, and K. V. Larin, "Quantification of molecular diffusion in arterial tissues with optical coherence tomography and fluorescence microscopy," *Laser Phys.*, vol. 19, pp. 1272–1275, 2009.
[62] K. V. Larin and V. V. Tuchin, "Functional imaging and assessment of the glucose diffusion rate in epithelial tissues with optical coherence tomography," *Quantum Electron.*, vol. 38, pp. 551–556, 2008.
[63] M. G. Ghosn, E. F. Carbajal, N. Befrui, A. Tellez, J. F. Granada, and K. V. Larin, "Permeability of hyperosmotic agent in normal and atherosclerotic vascular tissues," *J. Biomed. Opt.*, vol. 13, 010505, 2008.
[64] M. Ghosn, E. F. Carbajal, N. Befrui, V. V. Tuchin, and K. V. Larin, "Concentration effect on the diffusion of glucose in ocular tissues," *Opt. Lasers Eng.*, vol. 46, pp. 911–914, 2008.
[65] K. V. Larin, M. G. Ghosn, S. N. Ivers, A. Tellez, and J. F. Granada, "Quantification of glucose diffusion in arterial tissues by using optical coherence tomography," *Laser Phys. Lett.*, vol. 4, pp. 312–317, 2007.
[66] M. Ghosn, V. V. Tuchin, and K. V. Larin, "Depth-resolved monitoring of glucose diffusion in tissues by using optical coherence tomography," *Opt. Lett.*, vol. 31, pp. 2314–2316, 2006.
[67] M. G. Ghosn, V. V. Tuchin, and K. V. Larin, "Nondestructive quantification of analyte diffusion in cornea and sclera using optical coherence tomography," *Invest. Ophthalmol. Vis. Sci.*, vol. 48, pp. 2726–2733, Jun. 2007.
[68] M. G. Ghosn, M. Mashiatulla, S. H. Syed, M. A. Mohamed, K. V. Larin, and J. D. Morrisett, "Permeation of human plasma lipoproteins in human carotid endarterectomy tissues: Measurement by optical coherence tomography," *J. Lipid Res.*, vol. 52, no. 7, pp. 1429–1434, 2011.
[69] M. G. Ghosn, M. Mashiatulla, M. A. Mohamed, S. H. Syed, F. Castro-Chavez, J. D. Morrisett, and K. V. Larin, "Time dependent changes in aortic tissue during cold storage in physiological solution," *Biochim. Biophys. Acta.*, vol. 1810, pp. 555–560, 2011.
[70] L. S. de Melo, R. E. de Araujo, A. Z. Freitas, D. Zezell, N. D. Vieira, J. Girkin, A. Hall, M. T. Carvalho, and A. S. Gomes, "Evaluation of enamel dental restoration interface by optical coherence tomography," *J. Biomed. Opt.*, vol. 10, 064027, 2005.
[71] D. P. Popescu, M. G. Sowa, M. D. Hewko, and L. P. Choo-Smith, "Assessment of early demineralization in teeth using the signal attenuation in optical coherence tomography images," *J. Biomed. Opt.*, vol. 13(5), 054053, 2008.
[72] P. Wilder-Smith, L. Otis, J. Zhang, and Z. Chen, "Dental OCT," in *Optical Coherence Tomography*, W. Drexler and J. G. Fujimoto, Eds. Berlin, Germany: Springer, 2008, pp. 1151–1182.
[73] A. Kishen and S. Vedantam, "Hydromechanics in dentine: Role of dentinal tubules and hydrostatic pressure on mechanical stress-strain distribution," *Dent. Mater.*, vol. 23, pp. 1296–1306, Oct. 2007.
[74] C. T. Hanks, J. C. Fat, J. C. Wataha, and J. F. Corcoran, "Cytotoxicity and dentin permeability of carbamide peroxide and hydrogen peroxide vital bleaching materials, in vitro," *J. Dent. Res.*, vol. 72, pp. 931–938, May 1993.
[75] V. V. Tuchin, A. N. Bashkatov, E. A. Genina, V. I. Kochubey, V. V. Lychagov, S. A. Portnov, N. A. Trunina, D. R. Miller, S. Cho, H. Oh, B. Shim, M. Kim, J. Oh, H. Eum, Y. Ku, D. Kim, and Y. Yang, "Finger tissue model and blood perfused skin tissue phantom," *Proc. SPIE*, vol. 7898, pp. 78980Z-1–78980Z-10, 2011.
[76] M. Fujii, S. Yamanouchi, N. Hori, N. Iwanaga, N. Kawaguchi, and M. Matsumoto, "Evaluation of yucatan micropig skin for use as an in vitro model for skin permeation study," *Biol. Pharmaceutical Bulletin*, vol. 20, pp. 249–254, Mar. 1997.
[77] P. D. Agrba, M. Y. Kirillin, A. I. Abelevich, E. V. Zagaynova, and V. A. Kamensky, "Compression as a method for increasing the informativity of optical coherence tomography of biotissues," *Opt. Spectoscopy*, vol. 107, pp. 853–858, 2009.
[78] G. A. Askar'yan, "The increasing of laser and other radiation transport through soft turbid physical and biological media," *Soviet J. Quantum Electron.*, vol. 9, pp. 1379–1383, 1982.
[79] C. Drew, T. E. Milner, and C. G. Rylander, "Mechanical tissue optical clearing devices: Evaluation of enhanced light penetration in skin using optical coherence tomography," *J. Biomed. Opt.*, vol. 14(6), 064019, 2009.
[80] A. A. Gurjarpadhye, W. C. Vogt, Y. Liu, and C. G. Rylander, "Effect of localized mechanical indentation on skin water content evaluated using OCT," *Int. J. Biomed. Imag.*, vol. 2011, art. ID 817250, 2011.
[81] N. Guzelsu, J. F. Federici, H. C. Lim, H. R. Chauhdry, A. B. Ritter, and T. Findley, "Measurement of skin stretch via light reflection," *J. Biomed. Opt.*, vol. 8, pp. 80–86, Jan. 2003.
[82] A. P. Ivanov, S. A. Makarevich, and A. Y. Khairulina, "Propagation of radiation in tissues and liquids with densely packed scatterers," *J. Appl. Spectrosc.*, vol. 47, pp. 662–668, 1988.
[83] M. Y. Kirillin, P. D. Agrba, and V. A. Kamensky, "In vivo study of the effect of mechanical compression on formation of OCT images of human skin," *J. Biophotonics*, vol. 3, pp. 752–758, Dec. 2010.
[84] S. Nickell, M. Hermann, M. Essenpreis, T. J. Farrell, U. Kramer, and M. S. Patterson, "Anisotropy of light propagation in human skin," *Phys. Med. Biol.*, vol. 45, pp. 2873–2886, Oct. 2000.
[85] P. Rol, P. Niederer, U. Dürr, P.-D. Henchoz, and F. Fankhauser, "Experimental investigation on the light scattering properties of the human sclera," *Laser Light Ophthalmol.*, vol. 3, pp. 201–212, 1990.
[86] C. G. Rylander, O. F. Stumpp, T. E. Milner, N. J. Kemp, J. M. Mendenhall, K. R. Diller, and A. J. Welch, "Dehydration mechanism of optical clearing in tissue," *J. Biomed. Opt.*, vol. 11(4), 041117, 2006.
[87] H. Shangguan, S. Prahl, S. L. Jacques, L. W. Casperson, and K. W. Gregory, "Pressure effects on soft tissues monitored by changes in tissue optical properties," *Proc. SPIE*, vol. 3254, pp. 366–371, 1998.

[88] Y. P. Sinichkin, N. Kollias, G. Zonios, S. R. Utz, and V. V. Tuchin, "Reflectance and fluorescence spectroscopy of human skin in vivo," in *Optical Biomedical Diagnostics*, V. V. Tuchin, Ed. Bellingham, WA: SPIE Press, 2002, pp. 725–785.
[89] E. K. Chan, B. Sorg, D. Protsenko, M. O'Neil, M. Motamedi, and A. J. Welch, "Effects of compression on soft tissue optical properties," *IEEE J. Sel. Topics Quantum Electron.*, vol. 2, no. 4, pp. 943–950, Dec. 1996.
[90] M. A. Farage, K. W. Miller, P. Elsner, and H. I. Maibach, "Structural characteristics of the aging skin: A review," *Cutan Ocul. Toxicol*, vol. 26, pp. 343–357, 2007.
[91] C. S. Kim, P. Wilder-Smith, Y. C. Ahn, L. H. Liaw, Z. Chen, and Y. J. Kwon, "Enhanced detection of early-stage oral cancer in vivo by optical coherence tomography using multimodal delivery of gold nanoparticles," *J. Biomed. Opt.*, vol. 14(3), 034008, 2009.
[92] M. Kirillin, M. Shirmanova, M. Sirotkina, M. Bugrova, B. Khlebtsov, and E. Zagaynova, "Contrasting properties of gold nanoshells and titanium dioxide nanoparticles for optical coherence tomography imaging of skin: Monte Carlo simulations and *in vivo* study," *J. Biomed. Opt.*, vol. 14(2), 021017, 2009.
[93] A. K. Kohli and H. O. Alpar, "Potential use of nanoparticles for transcutaneous vaccine delivery: Effect of particle size and charge," *Int. J. Pharm.*, vol. 275, pp. 13–17, May 2004.
[94] X. Huang, P. K. Jain, I. H. El-Sayed, and M. A. El-Sayed, "Plasmonic photothermal therapy (PPTT) using gold nanoparticles," *Lasers Med. Sci.*, vol. 23, pp. 217–228, Jul. 2008.
[95] G. S. Terentyuk, G. N. Maslyakova, L. V. Suleymanova, N. G. Khlebtsov, B. N. Khlebtsov, G. G. Akchurin, I. L. Maksimova, and V. V. Tuchin, "Laser-induced tissue hyperthermia mediated by gold nanoparticles: Toward cancer phototherapy," *J. Biomed. Opt.*, vol. 14 (2), 021016, 2009.
[96] E. S. Tuchina and V. V. Tuchin, "TiO_2 nanoparticle enhanced photodynamic inhibition of pathogens," *Laser Phys. Lett.*, vol. 7, pp. 607–612, 2010.
[97] G. Cevc and U. Vierl, "Nanotechnology and the transdermal route: A state of the art review and critical appraisal," *J. Control Release*, vol. 141, pp. 277–299, Feb. 2010.
[98] J. Gupta, "Nanotechnology applications in medicine and dentistry," *J. Investigative Clinical Dentistry*, vol. 2, pp. 81–88, 2011.
[99] M.-H. Liu, C.-H. Chan, J.-H. Ling, and C. R. C. Wang, "Filling in dentinal tubules," *Nanotechnology*, vol. 18, pp. 475104-1–475104-6, 2007.
[100] A. Shrestha, S. W. Fong, B. C. Khoo, and A. Kishen, "Delivery of antibacterial nanoparticles into dentinal tubules using high-intensity focused ultrasound," *J. Endod.*, vol. 35, pp. 1028–1033, Jul. 2009.
[101] T. Suemori, J. Kato, T. Nakazawa, G. Akashi, and Y. Hirai, "A new nonvital tooth bleaching method using titanium dioxide and 3.5% hydrogen peroxide with a 405-nm diode laser or a halogen lamp," *Laser Phys. Lett.*, vol. 5, pp. 454–459, 2008.
[102] L. Li, H. Pan, J. Tao, X. Xu, C. Mao, X. Gu, and R. Tang, "Repair of enamel by using hydroxyapatitenanoparticles as the building blocks," *J. Mater. Chem.*, vol. 18, pp. 4079–4084, 2008.
[103] E. I. Galanzha, V. V. Tuchin, A. V. Solovieva, T. V. Stepanova, Q. Luo, and H. Cheng, "Skin backreflectance and microvascular system functioning at the action of osmotic agents," *J. Phys. D, Appl. Phys.*, vol. 36, pp. 1739–1746, 2003.
[104] E. Maeno, T. Shimizu, and Y. Okada, "Normotonic cell shrinkage induces apoptosis under extracellular low Cl conditions in human lymphoid and epithelial cells," *Acta. Physiol. (Oxf.)*, vol. 187, pp. 217–222, May/Jun. 2006.
[105] E. Genina, A. Bashkatov, Y. Sinichkin, and V. Tuchin, "Optical clearing of skin under action of glycerol: Ex vivo and in vivo investigations," *Opt. Spectrosc.*, vol. 109, pp. 225–231, 2010.
[106] D. Zhu, J. Zhang, H. Cui, Z. Mao, P. Li, and Q. Luo, "Short-term and long-term effects of optical clearing agents on blood vessels in chick chorioallantoic membrane," *J. Biomed. Opt.*, vol. 13(2), 021106, 2008.
[107] A. V. Zvyagin, X. Zhao, A. Gierden, W. Sanchez, J. A. Ross, and M. S. Roberts, "Imaging of zinc oxide nanoparticle penetration in human skin in vitro and in vivo," *J. Biomed. Opt.*, vol. 13(6), 064031, 2008.
[108] C. J. Murphy, A. M. Gole, J. W. Stone, P. N. Sisco, A. M. Alkilany, E. C. Goldsmith, and S. C. Baxter, "Gold nanoparticles in biology: Beyond toxicity to cellular imaging," *Acc. Chem. Res.*, vol. 41, pp. 1721–1730, Dec. 2008.
[109] R. Shukla, V. Bansal, M. Chaudhary, A. Basu, R. R. Bhonde, and M. Sastry, "Biocompatibility of gold nanoparticles and their endocytotic fate inside the cellular compartment: A microscopic overview," *Langmuir*, vol. 21, pp. 10644–10654, Nov. 2005.
[110] E. E. Connor, J. Mwamuka, A. Gole, C. J. Murphy, and M. D. Wyatt, "Gold nanoparticles are taken up by human cells but do not cause acute cytotoxicity," *Small*, vol. 1, pp. 325–327, Mar. 2005.
[111] T. Niidome, M. Yamagata, Y. Okamoto, Y. Akiyama, H. Takahashi, T. Kawano, Y. Katayama, and Y. Niidome, "PEG-modified gold nanorods with a stealth character for in vivo applications," *J. Control Release*, vol. 114, pp. 343–347, Sep. 2006.
[112] H. Takahashi, Y. Niidome, T. Niidome, K. Kaneko, H. Kawasaki, and S. Yamada, "Modification of gold nanorods using phosphatidylcholine to reduce cytotoxicity," *Langmuir*, vol. 22, pp. 2–5, Jan. 2006.

Kirill V. Larin received the first M.S. degree in laser physics and mathematics from the Saratov State University, Saratov, Russia, in 1995, the second M.S. degree in cellular physiology and molecular biophysics in 2001, and the Ph.D. degree in biomedical engineering in 2002 from the University of Texas Medical Branch, Galveston.

He is an Associate Professor of Biomedical Engineering at the University of Houston, Houston, TX. He is also with the Department of Physiology and Biophysics, Baylor College of Medicine, TX, and the Department of Optics and Biophysics at the Saratov State University, Saratov, Russia. He has authored more than 60 peer-reviewed publications and chapters in six books on Biomedical Optics. His research interests include biomedical optics and biophotonics and development and application of various optical methods for noninvasive and nondestructive imaging and diagnostics of tissues and cells.

Dr. Larin has received numerous awards including the Presidential Award from the Russian President Boris Yeltsin, the Wallace Coulter Young Investigator Translation Award, the Office of Naval Research Young Investigator Award, the Outstanding Young Investigator Award from the Houston Society for Engineers in Medicine and Biology, and the Herbert Allen Award from the American Society for Mechanical Engineers. He has delivered more than 50 invited and plenary talks, serves as a Cochair of Dynamics and Fluctuations in the Biomedical Photonics conference, and a member of number technical committees at professional conferences. He is also an Instructor for short courses on tissue optics and biophotonics for the SPIE, IEEE, and OSA.

Mohamad G. Ghosn received the B.S. degree in electrical and computer engineering and the M.S. degree in biomedical engineering both from and University of Houston, Houston, TX, in 2004 and 2006, respectively. He received the Ph.D. degree in biomedical engineering from the University of Houston in 2009.

He is a Postdoctoral Fellow at the Department of Medicine, Baylor College of Medicine, Houston TX. He has authored more than 15 peer-reviewed publications and two chapters in biomedical optics books. His main focus is the examination of molecular permeation of various drugs and analytes across biological tissues using optical coherence tomography.

Dr. Ghosn also enjoys teaching for which he was awarded the Outstanding Teacher Assistant Award for the year 2008 from the Cullen College of Engineering at the University of Houston.

Alexey N. Bashkatov received the Ph.D. degree in biophysics from Saratov State University, Saratov, Russia, in 2002.

He is the author or coauthor of more than 150 invited and contributed publications, six book chapters, and more than 200 invited and contributed presentations. Since 2002, he has been an Associate Professor in the Department of Optics and Biophotonics, Saratov State University. He is serving as a Referee by the *Journal of X-Ray Science and Technology, Biophysical Journal, BMC-Gastroenterology, JOSA A, Optics Express, Journal of Innovative Optical Health Sciences, Optics and Lasers in Engineering, Journal of Biophotonics, Ecological Modeling, Journal of Biomedical Optics, Optics Letters, Applied Optics, Biomedical Optics Express, Sensors, Journal of Quantitative Spectroscopy and Radiative Transfer, Optical Engineering, Quantum Electronics and Optics and Spectroscopy,* and is an Invitee Editor in the Journals of *Quantum Electronics and Optics and Spectroscopy of Russian Academy of Science*. His current research interests include study of optical properties of tissues, spectroscopy, development of methods for control of tissue absorption and scattering properties for medical optical diagnostics and therapy, modeling of light propagation in turbid media, and optical biophysics.

Elina A. Genina received the Ph.D. degree in biophysics from Saratov State University, Saratov, Russia, in 2002.

She is an Associate Professor in the Departments of Optics and Biophotonics, Saratov State University. She is the author or coauthor of more than 150 peer-reviewed publications and six book chapters on biomedical optics. She is serving as a Referee by the *Journal of Biomedical Optics*, *Journal of Innovative Optical Health Sciences*, *Quantum Electronics*, *Optics and Spectroscopy*, etc., and is an Invitee Editor in the *Journal of Innovative Optical Health Sciences*. She is a Scientific Secretary of International School for Junior Scientists and Students on optics, laser physics, and biophotonics (Saratov Fall Meeting). Her research interests include biomedical optics, laser medicine, and development of methods for control of tissue absorption and scattering properties for medical optical diagnostics and therapy.

Natalia A. Trunina received the Graduate degree (Hons.) from Saratov State University (SSU), Saratov, Russian, in 2009. She received the Master degree in physics in 2011. She is currently working toward the Ph.D. degree and an Engineer of the Department of Optics and Biophotonics, SSU.

She is a specialist in biochemical physics. She also takes part in the project Network of Excellence for Biophotonics (PHOTONICS4LIFE), a part of the Seventh Framework Program of Commission of the European Communities. She has published eight papers in scientific journals.

Ms. Natalia is a member of the International Society for Optics and Photonics and the Optical Society of America.

Valery V. Tuchin holds the Optics and Biophotonics Chair and is a Director of Research-Educational Institute of Optics and Biophotonics, Saratov State University, Saratov, Russia, and the Head of Laboratory on Laser Diagnostics of Technical and Living Systems, Institute of Precise Mechanics and Control, RAS. He has authored more than 300 peer-reviewed papers and books, including his latest *Tissue Optics: Light Scattering Methods and Instrumentation for Medical Diagnosis* (SPIE Press, 2nd ed., 2007), *Handbook of Optical Sensing of Glucose in Biological Fluids and Tissues* (CRC Press, Taylor & Francis Group, 2009), *Handbook of Photonics for Biomedical Science* (CRC Press, Taylor & Francis Group, 2010), and *Advanced Optical Cytometry: Methods and Disease Diagnoses* (Wiley-VCH Verlag GmbH & Co. KGaA, 2011). His research interests include biophotonics, biomedical optics, laser medicine, and physics of optical and laser measurements.

Dr. Tuchin has been awarded title "Honored Science Worker of the Russian Federation" and became a fellow of the SPIE; he is a Vice President of the Russian Photobiology Society. In 2007, he was awarded the SPIE Educator Award. He is a FiDiPro Professor (Finland Distinguished Professor Program, awarded by TEKES for the period 2011–2014).